Geosci. Model Dev., 3, 689–716, 2010
www.geosci-model-dev.net/3/689/2010/
doi:10.5194/gmd-3-689-2010

Geoscientific Model Development

Modeling global atmospheric CO_2 with improved emission inventories and CO_2 production from the oxidation of other carbon species

R. Nassar[1,2,*], D. B. A. Jones[1], P. Suntharalingam[3], J. M. Chen[2], R. J. Andres[4], K. J. Wecht[5], R. M. Yantosca[6], S. S. Kulawik[7], K. W. Bowman[7], J. R. Worden[7], T. Machida[8], and H. Matsueda[9]

[1]Department of Physics, University of Toronto, 60 St. George Street, Toronto, Ontario, M5S 1A7, Canada
[2]Department of Geography, University of Toronto, 45 St. George Street, Toronto, Ontario, M5S 2E5, Canada
[3]Environmental Sciences, University of East Anglia, Norwich, NR4 7TJ, UK
[4]Environmental Sciences Division, Oak Ridge National Laboratory, Oak Ridge, TN, 37831-6335, USA
[5]Department of Earth and Planetary Sciences, Harvard University, Pierce Hall, 29 Oxford St., Cambridge, MA, 02138, USA
[6]School of Engineering and Applied Sciences, Harvard University, Pierce Hall, 29 Oxford St., Cambridge, MA, 02138, USA
[7]Jet Propulsion Laboratory, California Institute of Technology, 4800 Oak Grove Drive, Pasadena, CA, 91109, USA
[8]National Institute for Environmental Studies, 16-2 Onogawa, Tsukuba-City, Ibaraki, 305-8506, Japan
[9]Meteorological Research Institute, 1-1 Nagamine, Tsukuba-City, Ibaraki 305-0052, Japan
[*]now at: Climate Research Division, Environment Canada, 4905 Dufferin St., Toronto, Ontario, M3H 5T4, Canada

Received: 5 June 2010 – Published in Geosci. Model Dev. Discuss.: 2 July 2010
Revised: 8 October 2010 – Accepted: 24 November 2010 – Published: 15 December 2010

Abstract. The use of global three-dimensional (3-D) models with satellite observations of CO_2 in inverse modeling studies is an area of growing importance for understanding Earth's carbon cycle. Here we use the GEOS-Chem model (version 8-02-01) CO_2 mode with multiple modifications in order to assess their impact on CO_2 forward simulations. Modifications include CO_2 surface emissions from shipping ($\sim 0.19\,\mathrm{Pg\,C\,yr^{-1}}$), 3-D spatially-distributed emissions from aviation ($\sim 0.16\,\mathrm{Pg\,C\,yr^{-1}}$), and 3-D chemical production of CO_2 ($\sim 1.05\,\mathrm{Pg\,C\,yr^{-1}}$). Although CO_2 chemical production from the oxidation of CO, CH_4 and other carbon gases is recognized as an important contribution to global CO_2, it is typically accounted for by conversion from its precursors at the surface rather than in the free troposphere. We base our model 3-D spatial distribution of CO_2 chemical production on monthly-averaged loss rates of CO (a key precursor and intermediate in the oxidation of organic carbon) and apply an associated surface correction for inventories that have counted emissions of CO_2 precursors as CO_2. We also explore the benefit of assimilating satellite observations of CO into GEOS-Chem to obtain an observation-based estimate of the CO_2 chemical source. The CO assimilation corrects for an underestimate of atmospheric CO abundances in the model, resulting in increases of as much as 24% in the chemical source during May–June 2006, and increasing the global annual estimate of CO_2 chemical production from 1.05 to 1.18 Pg C. Comparisons of model CO_2 with measurements are carried out in order to investigate the spatial and temporal distributions that result when these new sources are added. Inclusion of CO_2 emissions from shipping and aviation are shown to increase the global CO_2 latitudinal gradient by just over 0.10 ppm (~3%), while the inclusion of CO_2 chemical production (and the surface correction) is shown to decrease the latitudinal gradient by about 0.40 ppm (~10%) with a complex spatial structure generally resulting in decreased CO_2 over land and increased CO_2 over the oceans. Since these CO_2 emissions are omitted or misrepresented in most inverse modeling work to date, their implementation in forward simulations should lead to improved inverse modeling estimates of terrestrial biospheric fluxes.

1 Introduction

An important application of global three-dimensional (3-D) modeling of atmospheric carbon dioxide (CO_2) is the assimilation of CO_2 observations to obtain optimized estimates of atmospheric CO_2 distributions or CO_2 surface

Correspondence to: R. Nassar
(ray.nassar@ec.gc.ca)

Published by Copernicus Publications on behalf of the European Geosciences Union.

fluxes (source/sink strengths). The optimization of CO_2 fluxes (also referred to as inverse modeling) has mainly been carried out using in situ or flask observations obtained near the surface of the Earth, but in recent years, many studies have explored the potential of inverse modeling using satellite observations (Pak and Prather, 2001; Rayner and O'Brien, 2001; Houweling et al., 2004, 2010; Miller et al., 2007; Chevallier et al., 2007; Kadygrov et al., 2009). A significant challenge with the inverse modeling approach is that inferred flux estimates are sensitive to systematic errors in the models and observations (Miller et al., 2007; Chevallier et al., 2007; Kadygrov et al., 2009; Houweling et al., 2010) and since satellite observations measure atmospheric columns or profiles rather than point measurements at the Earth's surface, the 3-D representation of CO_2 in the model is of increased importance. Reducing spatially-dependent biases in the models requires not only a better representation of atmospheric transport and surface sources and sinks of CO_2, but also the inclusion of 3-D sources distributed throughout the troposphere, such as emission of CO_2 from aviation and the chemical production of CO_2 from the oxidation of CO, CH_4 and other carbon gases. The importance of accounting for this tropospheric chemical source of CO_2 in models has previously been acknowledged (Enting and Mansbridge, 1991; Enting et al., 1995; Baker, 2001; Enting, 2004; Folberth et al., 2005; Suntharalingam et al., 2005; Denman et al., 2007, Ch. 7 IPCC-AR4). To balance atmospheric CO_2 in the absence of this 3-D chemical source, many inventories count CO_2 precursor species (CO, CH_4 and other carbon gases) as direct CO_2 emissions at the surface, leading to a reasonable estimate of total CO_2 over time, but an incorrect spatial distribution, since real chemical production of CO_2 from these species occurs at different times and locations from emission. Model implementation of CO_2 chemical production therefore also requires adjustments to surface emission inventories that use this approach. Since chemical production of CO_2 is greatest in the tropics, while most surface emissions occur in the Northern Hemisphere, the combined chemical production and surface correction will have an impact on the global latitudinal gradient of CO_2, which is an indentified weakness of CO_2 models (Law et al., 1996; Taylor and Orr, 2000; Gurney et al., 2003) and consequently could affect inverse modeling estimates of CO_2 fluxes.

In this work, we use the GEOS-Chem CO_2 simulation with multiple modifications applied to investigate the impact of these changes on atmospheric CO_2 distributions. This work is motivated by our objective of improving CO_2 forward simulations for use in inverse modeling with satellite observations of CO_2. Our modifications to the CO_2 simulation include improved temporal variability in the national surface fossil fuel combustion and cement manufacture inventory, the addition of surface CO_2 emissions from shipping, 3-D CO_2 emissions from domestic and international aviation, and 3-D chemical production of CO_2 from the oxidation of reduced carbon species, along with an associated surface correction. Although a small number of past forward or inverse modeling studies have included CO_2 chemical production (Enting and Mansbridge, 1991; Enting et al., 1995; Baker, 2001), to the best of our knowledge, our modifications result in the most comprehensive online model representation of 3-D CO_2 chemical production and the appropriate surface correction in forward simulations. Use of the resulting model distributions in inverse analyses enables a significant reduction in the systematic error introduced into surface CO_2 flux estimates through the misallocation of the reduced carbon fluxes. We base our CO_2 chemical source on the rates of conversion of CO to CO_2 from GEOS-Chem simulations of tropospheric ozone-hydrocarbon chemistry. We also briefly explore the assimilation of satellite observations of CO from the Tropospheric Emission Spectrometer (TES) into GEOS-Chem to produce an optimized CO distribution, from which we obtain an observationally-based estimate of the chemical production of CO_2.

The impact on our model simulations of these newly-added inventories and our representation of CO_2 chemical production is quantified and the simulations are compared with GLOBALVIEW-CO_2 (GLOBALVIEW, 2009) and CONTRAIL aircraft flask measurements (Matsueda et al., 2002, 2008; Machida et al., 2008). It is important to emphasize that in this work we have focused our model improvement efforts on better representing emissions related to fossil fuel use (on land, from shipping, aviation, and chemical production related to emission of CO_2 precursors), rather than addressing the representation of biospheric CO_2 fluxes in the model. This choice was deliberate, since CO_2 inverse modeling studies typically fix fossil fuel emissions assuming highly accurate inventories, while land biospheric CO_2 fluxes (which have larger uncertainties) are optimized using inverse modeling. This approach is currently being applied to our inverse modeling to obtain improved biospheric flux estimates using CO_2 observations from the TES satellite instrument and from the surface observational network (Nassar et al., 2010).

2 GEOS-Chem CO_2 simulation

GEOS-Chem is a global chemical transport model (CTM) that uses GEOS (Goddard Earth Observing System) assimilated meteorological fields from the NASA Global Modeling and Assimilation Office (GMAO). The model has multiple separate simulation modes, the most common of which is the O_x-NO_x-hydrocarbon chemistry or "full chemistry" mode (Bey et al., 2001). This mode has been extensively validated using in situ and satellite observations (e.g. Li et al., 2004; Folkins et al., 2006; Nassar et al., 2009; Kopacz et al., 2010; Millet et al., 2010). An early version of the CO_2 mode is described in Suntharalingam et al. (2004),

Table 1. Summary of key inventories for GEOS-Chem CO_2 simulations in this work along with global total values in Pg C yr^{-1} for one or more simulation years.

Flux Type	Inventory Name/ Abbreviation	Description	Global Annual Flux	References
National fossil fuel and cement manufacture	CDIAC $1^\circ \times 1^\circ$ monthly	$1^\circ \times 1^\circ$ monthly fossil fuel and cement manufacture CO_2 emissions from national totals for 1950–2006 and scaled for 2007–2009 (excludes international bunker fuels)	1.63–8.67 Pg C yr^{-1}, 8.23 Pg C yr^{-1} (2006)	Andres et al. (2010)
Biomass Burning	GFEDv2	$1^\circ \times 1^\circ$ biomass burning CO_2 emissions: monthly for 1991–2008 or 8-day averages for 2001–2007	1.88-3.12 Pg C yr^{-1}, 2.16 Pg C yr^{-1} (2006)	van der Werf et al. (2006)
Biofuel Burning	Yevich & Logan	$1^\circ \times 1^\circ$ annual inventory of biofuel (heating/cooking) CO_2 emissions for 1985 and scaled to 1995, excluding burning in agricultural fields	0.80 Pg C yr^{-1} (1995)	Yevich and Logan (2003)
Ocean Exchange	Takahashi et al. (2009)	$4^\circ \times 5^\circ$ climatology of monthly ocean-atmosphere CO_2 flux	–1.41 Pg C yr^{-1}	Takahashi et al. (2009)
Balanced Biosphere	CASA	$1^\circ \times 1^\circ$ 3-hourly Net Ecosystem Productivity (NEP) for 2000	0.00 Pg C yr^{-1}	Olsen and Randerson (2004)
Residual Annual Terrestrial Exchange	TransCom climatology	$1^\circ \times 1^\circ$ annual climatology based on TransCom CO_2 inversion results adjusted with GFEDv2 fire emissions	–5.29 Pg C yr^{-1}	Baker et al. (2006), van der Werf et al. (2006)
Shipping	ICOADS	$0.1^\circ \times 0.1^\circ$ monthly shipping emissions of CO_2 scaled for 1985–2009	0.12–0.20 Pg C yr^{-1}, 0.19 Pg C yr^{-1} (2006)	Corbett and Koehler (2003, 2004), Endresen et al. (2004, 2007)
Aviation	AEAP-SAGE	$2^\circ \times 2.5^\circ$ gridded flight track density based on Friedl (1997) used for GEOS-Chem sulfate simulation scaled to 1985–2006 for aviation CO_2 emissions	0.12–0.18 Pg C yr^{-1}, 0.16 Pg C yr^{-1} (2006)	Friedl (1997), Sausen and Schuman (2000), Kim et al. (2005, 2007), Wilkerson et al. (2010)
Chemical Source	GEOS-Chem CO_2 Chemical Source	Chemical production of CO_2 based on CO loss rates from GEOS-Chem $4^\circ \times 5^\circ$ simulations (GEOS-4 2000–2006, GEOS-5 2006–2009)	1.04–1.06 Pg C yr^{-1}, 1.05 Pg C yr^{-1} (2006)	This work

which contained no chemistry but included atmospheric CO_2 fluxes from biomass burning, biofuel burning, fossil fuel burning and cement manufacture, ocean exchange and terrestrial biospheric exchange described in Suntharalingam et al. (2003). Previous application of this version of the model for inverse modeling of atmospheric CO_2 is described in Palmer et al. (2006), Miller et al. (2007), Feng et al. (2009), Wang et al. (2009) and Feng et al. (2010). In this work, we use version 8-02-01 of GEOS-Chem to assess the impact of the new inventories and the oxidation source on the CO_2 simulation. The following subsections describe components of the CO_2 simulation that are used in this work and are available in GEOS-Chem v8-03-02 or later. The preferred inventory choices, which are used for most simulations in this work are summarized in Table 1.

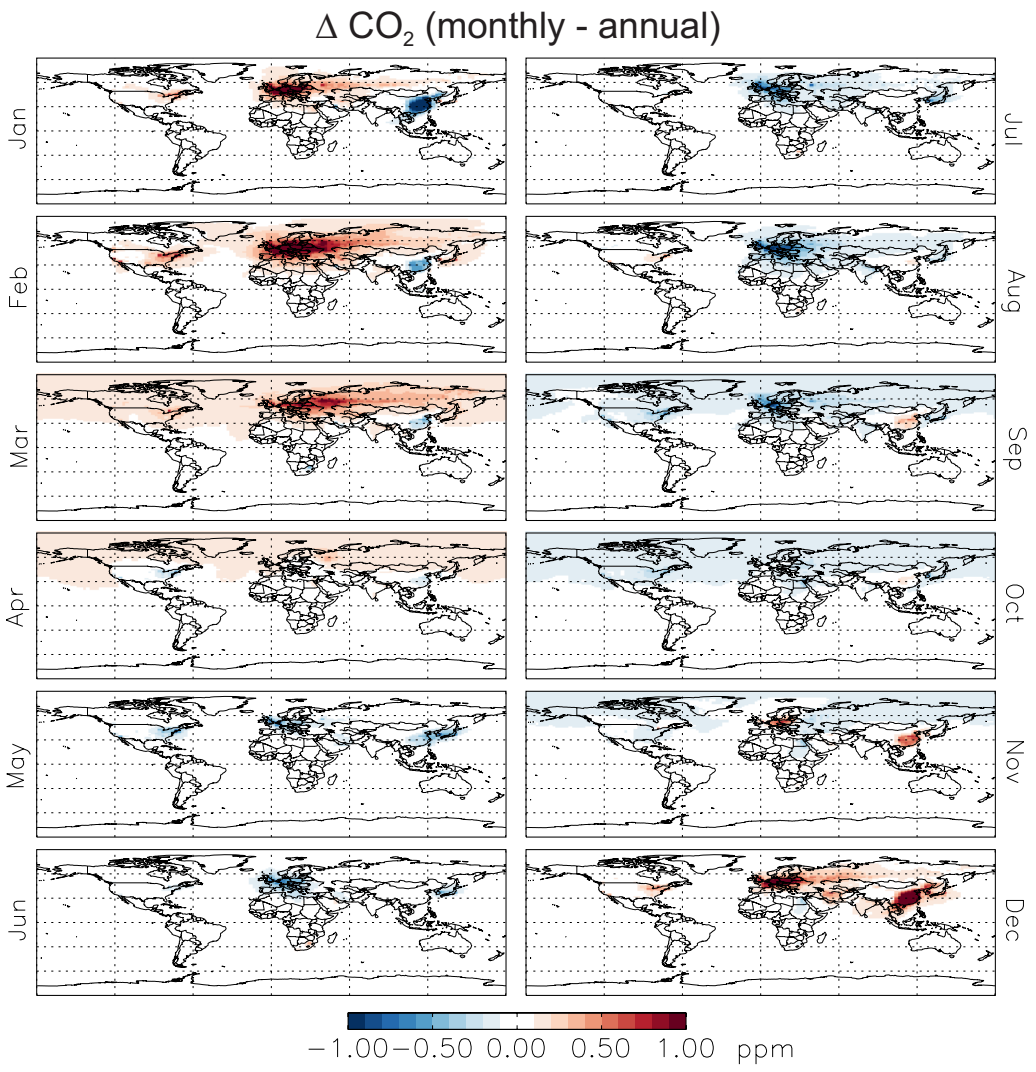

Fig. 1. Comparison of monthly-averaged surface level CO_2 in 2006 from a simulation using the monthly-varying fossil fuel emissions and another simulation using annual fossil fuel emissions with the same cumulative annual total. The simulations began with the same initial conditions for 1 January 2006 and were identical in all other respects.

2.1 Fossil fuel burning and cement manufacture

The original version of the GEOS-Chem CO_2 simulation used global annual emissions of CO_2 from fossil fuels and cement manufacture for 1995 at $1° \times 1°$ resolution (Andres et al., 1996), regridded offline to the GEOS grids. The inventory was developed at the Carbon Dioxide Information and Analysis Centre (CDIAC) of the Oak Ridge National Laboratory (ORNL) based on reported national CO_2 emissions for 186 countries, which were spatially distributed using detailed population statistics (United Nations, 1984) and national political boundaries from the Goddard Institute for Space Studies (GISS). The earlier version of the inventory corresponded to the first year of each decade from 1950–1990 but has since been expanded and improved such that the current version spans 1950–2006, providing monthly emission totals to account for the differing regional seasonal variability of fossil fuel use related to climate and economic factors (Andres et al., 2010). This updated inventory is important since global fossil fuel emissions have been increasing significantly since the 1990s, contributing 8.23 Pg C in 2006. Also included in this inventory is the non-fossil fuel production of CO_2 from cement manufacture, which occurs via the conversion of $CaCO_3$ to $CaO + CO_2$, representing about 5% of total emissions in the inventory, but a larger proportion in China, the world's highest emitting nation.

Figure 1 shows monthly surface CO_2 comparisons between GEOS-Chem runs with monthly and annually varying fossil fuel emissions, starting from the same initial conditions. The monthly-varying emissions lead to more CO_2 in the Northern Hemisphere (NH) in the first few

months of the year, driven by high fossil fuel use in Europe, Canada and the northern United States, presumably related to winter heating. Although the difference during the NH winter is largest over northern populated areas where it exceeds 1 ppm, the background CO_2 is also elevated by about 0.1 ppm from 30–90° N in March. In NH spring, heating requirements are reduced, and by May, the elevated CO_2 mostly disappears since springtime fossil fuel emissions from Europe, Canada and the northern US are below the annual average. In July and August, European fossil fuel emissions remain below their annual mean, while the US northeast is slightly above, presumably due to elevated energy consumption from air-conditioning use. In September and October, NH CO_2 is lower than the annual average (nearly mirroring March and April) since energy consumption due to heating and cooling reaches an annual minimum. At the end of the year, the run with monthly emissions returns to higher CO_2 values over Europe and the US.

The observed seasonality over China is markedly different from other high-emitting regions. Rather than exhibiting the cyclical pattern of Europe, the US and Canada, a near-constant increase is the dominant form of change observed over China. The increase in CO_2 emissions from China over the course of a single year, captured by the monthly inventory (but not the annual one) has an impact comparable in magnitude to the seasonal cycle from other high-emitting regions. Therefore, in addition to masking the seasonality of emissions (related to seasonally-varying energy consumption based on heating and air conditioning), an annual rather than monthly inventory would represent the fairly constant increase in CO_2 emissions from China (Gregg et al., 2008) as an unrealistically abrupt jump on 1 January of each year.

Overall, this comparison indicates that a fossil fuel inventory based on monthly totals rather than annual totals has an impact often exceeding 1.0 ppm near the surface over regions of high fossil fuel consumption (Europe, US, Canada and China). Away from the source regions, the impact is muted, decreasing to about 0.1 ppm across the NH. The differences are negligible in the tropics and Southern Hemisphere (SH).

Preliminary fossil fuel data for 2007 and 2008 for major emitting countries (based on BP energy statistics) were used to scale the monthly spatial distributions of 2006, based on estimated ratios for these years relative to 2006 values, such that the seasonality in the emissions remains unchanged. Ratios were applied at the national level for the US, Canada, Mexico, Australia, China, India and Japan. The rest of the world was scaled by regions: South/Central America and the Caribbean, Africa, the Middle East, Europe and the former Soviet Union, and Asia-Pacific. Le Quéré et al. (2009) estimate that 2009 global fossil fuel emissions were 2.8% less than 2008 levels or slightly below 2007, so we apply scaling factors for 2009 based on scaling factors for 2007, except for the US, Australia and China. US emissions decreased by 3.1% from 2007 to 2008, so we apply a similar decrease for 2009. Australia's emission also decreased from 2007 to 2008, so we simply apply the lower 2008 values. China's emissions increased by 15.5% from 2006 to 2008 roughly equally for both years, but to balance the total sum of all nations, we reduced 2009 emissions from China to 9% above 2006 levels. Based on new CDIAC monthly data (Andres et al., 2010) for 2007 and recent updated global estimates (Friedlingstein et al., 2010), our scaling is no longer needed for 2007 and will be revisited for subsequent years.

2.2 Biomass burning

Biomass burning includes the burning of vegetation induced by natural processes like lightning as well as anthropogenically-induced burning, a common method of clearing vegetation for agriculture or urbanization. GEOS-Chem can be run with climatological, seasonally-varying biomass burning emissions (Duncan et al., 2003) or the much preferred year-specific Global Fire Emission Database version 2 (GFEDv2) (van der Werf et al., 2006). The GFEDv2 approach is to apply a CO_2 emission factor for each vegetation type (savanna, tropical forest, extratropical forest) to a fuel load and burned area determined from MODIS (Moderate Resolution Imaging Spectroradiometer) 8-day fire counts (Giglio et al., 2003). GFEDv2 CO_2 emission data are provided at $1^\circ \times 1^\circ$ and regridded during a GEOS-Chem simulation. GFEDv2 is available as monthly averages (1997–2008) or 8-day averages (2001–2007). The mean global annual CO_2 in GFEDv2 (1997–2008) is 2.35 Pg C yr^{-1} (approximately 30% of CO_2 from fossil fuel combustion), thus it represents a significant source of CO_2. A model update will soon be available permitting simulations to use GFEDv3 (van der Werf et al., 2010) for 1997–2009.

2.3 Biofuel burning

Biofuel burning in this context refers to the anthropogenic burning of vegetation for heating, cooking and removal of agricultural waste, mostly in developing countries. The model uses annual mean biofuel CO_2 emissions from Yevich and Logan (2003) with a native resolution of $1^\circ \times 1^\circ$. The global annual sum of the biofuel CO_2 emissions in this inventory is 0.9 Pg C for 1985, however, the component of the inventory from agricultural burning in fields is not included since this is better represented by GFED, yielding 0.73 Pg C. We scale 1985 values to 1995 according to Yevich and Logan (2003), giving a total without burning in fields of 0.80 Pg C. Growth patterns of global biofuel emissions beyond 1995 are unclear, but a steady increase is unlikely due to a shift to fossil fuels in the developing world as urbanization increases. No diurnal or seasonal variability or trends in biofuel emissions are included, but since the biofuel contribution is small relative to other sources, the error in assuming constant emissions from 1995 should also be small.

2.4 Terrestrial biospheric exchange

Terrestrial biospheric exchange in the model consists of two components. The first is referred to as the "balanced biosphere" and is based on the Carnegie-Ames-Stanford-Approach (CASA) model (Potter et al., 1993; Randerson et al., 1997). For the specific CASA run used here (Olsen and Randerson, 2004), the sum of the Gross Primary Production (GPP) and ecosystem respiration (R_e) is taken to represent Net Ecosystem Productivity (NEP) for 2000. Monthly mean NEP fluxes from CASA were interpolated to daily values and balanced such that they give no net annual uptake/release of CO_2. In balancing the CASA fluxes, the net global contribution is set to 0 Pg C yr^{-1} in order to represent terrestrial fluxes with no anthropogenic interference. These CASA balanced biosphere fluxes implicitly account for the natural cycle of non-respiratory carbon losses from the biosphere such as fires, methane and NMVOCs, and leaching of soil organic carbon (Randerson et al., 2002). The CASA NEP output is used as Net Ecosystem Exchange (NEE) in our model simulation. Although these NEE balanced biosphere fluxes contribute no net annual uptake/release of CO_2 by design, they make the largest contribution to the seasonal cycle of atmospheric CO_2 over both land and ocean over most of the globe with the greatest impacts (largest amplitude) seen in the Northern Hemisphere. A representation of the diurnal cycle is also included with the NEP interpolated to eight 3-h intervals each day (Olsen and Randerson, 2004).

A second component for CO_2 resulting from terrestrial biospheric exchange is necessary to account for the total annual sum of biospheric uptake and emission of CO_2, which we refer to as the residual annual terrestrial exchange. This biospheric flux term is commonly the state to be optimized in inverse modeling. To provide a good a priori description of this residual annual terrestrial exchange for inverse modeling, we have incorporated into the model a climatology of inversion results from TransCom 3 (Baker et al., 2006), applied for the 11 TransCom land regions, as shown in Fig. 2. In TransCom, the residual annual biospheric flux is defined to include GPP and R_e as well as biomass burning, unlike in GEOS-Chem where burning is primarily specified separately. Since biofuel emissions were not explicitly dealt with in the TransCom inversions, they will also have been implicitly included in their residual annual terrestrial exchange. To account for this, we subtract a GFEDv2 climatology and 1995 biofuel burning emissions from the TransCom climatology to obtain an estimate of the NEE component only. The TransCom climatology spans the years 1991–2000. For the GFED climatology, we use 1997–2006 (with a standard deviation of 15%), thus both decade-long periods include the strong Southeast Asian biomass burning event related to the 1997–1998 El Niño, that resulted in global CO_2 emissions that were 23% higher than average in 1997 and 30% higher in 1998. Biomass burning emissions

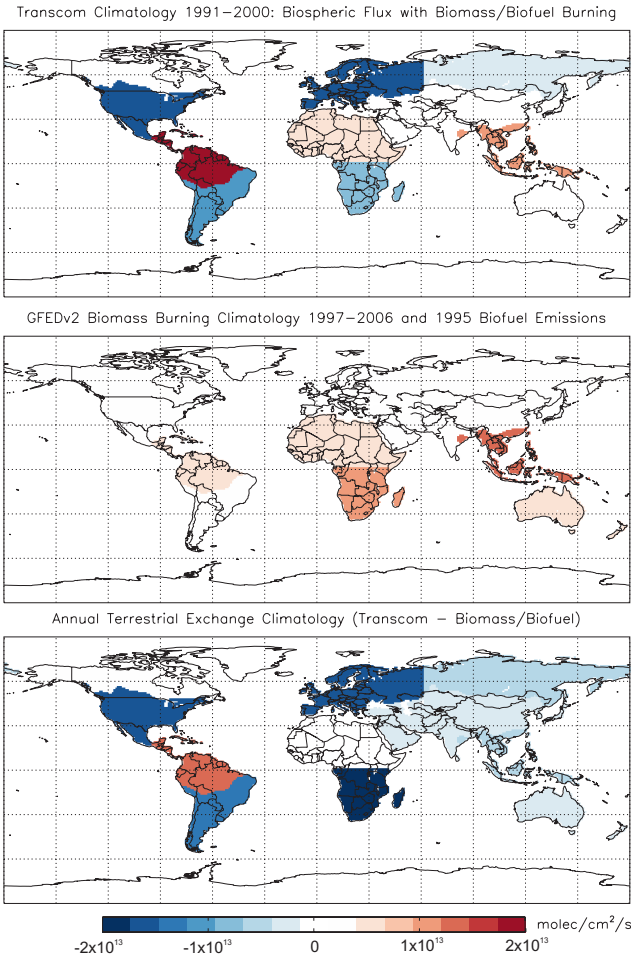

Fig. 2. Annual terrestrial exchange from Baker et al. (2006) for a climatology representing 1991–2000, with values distributed equally within each of the 11 TransCom3 land regions (top). Sum of GFEDv2 climatology of biomass burning emissions for 1997–2006 with biofuel burning emissions for 1995 distributed as in the previous panel (middle). Combination of two earlier panels giving the constant annual terrestrial exchange in the model (bottom).

were available from GFEDv2 for 2007–2008, but these were left out of the climatology to avoid "dilution" of the strong El Niño signal in one climatology but not the other.

With the climatological approach to terrestrial biospheric fluxes, the problem of double-counting natural biomass burning processes (which are in both CASA and GFED), is mitigated since the inversion result optimizes the sum of these terms. An acknowledged weakness in this climatological approach is the gradual downward trend in global biomass burning emissions in GFED over this time period, coupled with the inferred upward trend in NEE annual terrestrial flux which has maintained a near constant CO_2 airborne fraction while fossil fuel CO_2 emissions have risen (Gloor et al., 2010).

The direct TransCom climatology (Baker et al., 2006) gives an average of –2.09 Pg C yr^{-1} for residual terrestrial sinks, the GFED climatology (van der Werf et al., 2006) gives an average of +2.39 Pg C yr^{-1}, and biofuel emissions were +0.80 Pg C yr^{-1}, which when combined gives a climatology with a global total of –5.29 Pg C yr^{-1} (Fig. 2). Relative to net annual terrestrial exchange in the previous version of GEOS-Chem, the climatology has an opposite sign for the flux over Temperate North America (now a sink as shown by others) and Tropical America goes from near neutral to a source. The performance of the forward model with this a priori annual net exchange is evaluated in Sect. 3 and its performance in inverse modeling will be evaluated in Nassar et al. (2010).

2.5 Ocean exchange

GEOS-Chem simulates ocean release and uptake of CO_2 using ocean climatologies. The original GEOS-Chem CO_2 simulation relied on the ocean climatology from Takahashi et al. (1997), which was based on about 250 000 non-El Niño measurements of the pressure of CO_2 dissolved in ocean water (pCO_2), globally interpolated to an annual mean $4^\circ \times 5^\circ$ ocean grid, with a unit conversion (to molecules of CO_2 cm^{-2} s^{-1}) applied and regridded to the GEOS grids. An improved version of the ocean climatology with monthly variability was later developed (Takahashi et al., 2002). The most recent version, based on 3 million non-El Niño pCO_2 measurements (Takahashi et al., 2009) has now been implemented in GEOS-Chem, with the option of selecting an annual mean or monthly-varying climatology. The tropical oceans (especially the equatorial eastern Pacific) are generally a CO_2 source, while the mid- and high-latitude oceans (especially the north Atlantic) are generally a CO_2 sink. The main exceptions are CO_2 source regions along the Antarctic sea ice-ocean boundary and a small, variable source near the Bering Sea. The new climatology obtained from Takahashi et al. (2009) indicates a net global annual ocean flux of -1.4 ± 0.3 Pg C yr^{-1}, a somewhat stronger sink estimate than that from Takahashi et al. (1997). It should be noted that the above number represents only the ocean-atmosphere CO_2 flux and not the total ocean carbon sink which includes lateral contributions to the ocean from rivers. Takahashi et al. (2009) quote a riverine contribution of 0.45 Pg C yr^{-1} (from Jacobson et al., 2007a) for comparing with ocean carbon sink estimates, but other estimates of the global riverine component are as high as 0.90 Pg C yr^{-1} (Cole et al., 2007). The riverine carbon contribution to the ocean is only significant when comparing an ocean-atmosphere flux with ocean carbon sinks, since this indirect transfer of atmospheric carbon to the ocean via the land, is treated as a component of the land sink in GEOS-Chem and in atmospheric inverse modeling.

2.6 Shipping and aviation

Due the fact that the national CO_2 emission sums that are spatially distributed in the CDIAC $1^\circ \times 1^\circ$ inventory (Andres et al., 1996, 2010) are primarily intended to show national origin of emissions, the inventory does not include CO_2 emissions from bunker fuels. These fuels are considered international (not associated with any specific nation) since they are predominantly used for international shipping and aviation. (One exception is the CO_2 emission from Antarctic fisheries, which is treated as a separate national inventory.) For example, global annual CO_2 emissions from fossil fuels in 2006 (from CDIAC) amounted to 8.230 Pg C, but the sum of national emissions amounted to 7.828 Pg C yielding a difference of 0.402 Pg C of which 0.255 Pg C is attributed to bunker fuels. The remainder of the difference primarily relates to non-combustion uses of fossil fuels such as the chemical production of plastics, with a smaller contribution (positive or negative) from changes in fuel reserves from year to year.

Accounting for CO_2 emissions from shipping and aviation in the model requires knowledge of both the quantity and spatial distribution of emissions. The spatial distribution of shipping emissions based on the Emissions Database for Global Atmospheric Research (EDGAR) v2.0 inventory (Olivier and Berdowsky, 2001) is now an option for CO_2 (as for other chemical species in GEOS-Chem), but it contains a largely simplified representation of shipping routes. More updated versions of EDGAR ship emissions are expected to be better, however, EDGAR v3.0, the Automated Mutual-assistance Vessel Rescue system (AMVER) and the International Comprehensive Ocean-Atmosphere Data Set (ICOADS) shipping distributions are compared in Eyring et al. (2010), suggesting that ICOADS is the most realistic. A detailed accounting of emissions from ship traffic based on ICOADS has been developed by Corbett and Koehler (2003, 2004), which is available globally at $0.1^\circ \times 0.1^\circ$ horizontal resolution with monthly variability. The global annual emissions sum in Corbett and Koehler (2003) has been disputed by Endersen et al. (2004), leading to some revisions (Corbett and Koehler, 2004); however, no significant issues with the distribution have been identified. The global annual sum of shipping emissions that we obtain from the inventory is 176 Tg C. In our implementation of the inventory in the model for CO_2, we scale the distribution to annual values as follows. We determine the linear trend in emissions using 1985, 1990, 1995, 2000 and 2002 values from Endresen et al. (2007). We then determine values for all years in the 1985–2008 range based on the slope and intercept of this trend. For 2009, values for 2007 are used for consistency with the decline in global fossil fuel combustion associated with a reduction in international trade (Le Quéré et al., 2009). For ship emissions related to international bunker fuel consumption, there is no significant duplication of emission with the main fossil fuel source in the model. Some shipping,

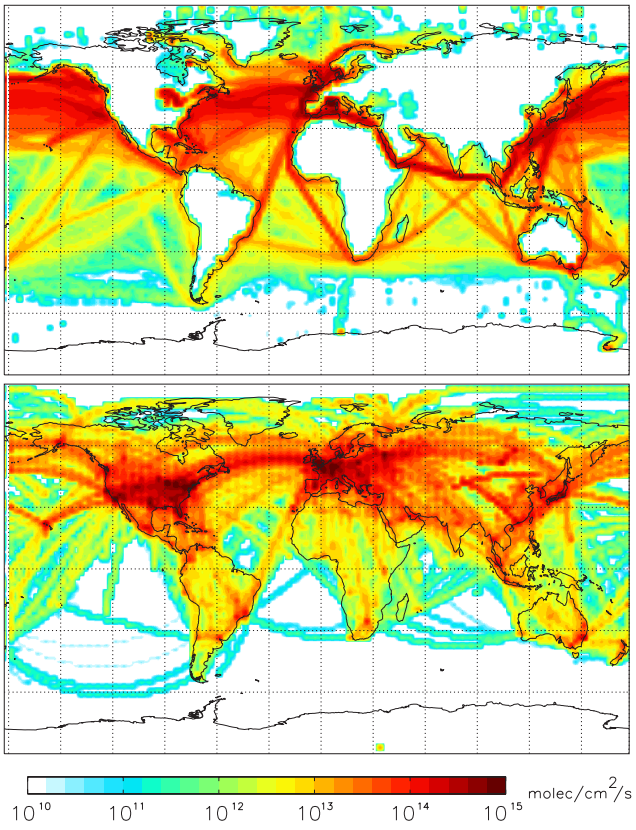

Fig. 3. CO_2 emissions from international shipping for the year 2006 (top). CO_2 emissions from international and domestic aviation for the year 2006 (bottom).

especially close to shorelines could be from domestic trade, but this likely amounts to less than 15% (Endresen et al., 2003). Figure 3 shows the annual CO_2 emissions in the model from shipping on a log scale for 2006, which clearly exhibits higher emissions over the oceans of the NH.

Emissions from aviation have been included in the GEOS-Chem sulfate simulation based on a 3-D distribution of emissions from the Atmospheric Effects of Aviation Project (AEAP) (Friedl, 1997). More recent studies by the System for Assessing Aviation Emissions (SAGE) (Kim et al., 2005, 2007) have continued to analyze the impact of aviation emissions. According to the SAGE assessment, the mean vertical profile of global aviation emissions has a small peak in the lowest kilometer (where takeoff and landing occur), is uniformly low between 1–9 km, and has a large peak from 9–12 km, with essentially no emissions above 12 km. Aviation emissions are most intense over the continental US, Europe and parts of Asia, as well as the flight paths over the oceans connecting these regions, while emissions in the SH are comparatively low. Sausen and Schumann (2000) provide a table of global annual emissions up to 1995, which we use to scale the AEAP distribution for each year beginning in 1985 at 123 Tg C to 154 Tg C in 1995. Kim et al. (2007) show a continued rise from 156 to 175 Tg C from 2000 to 2005, although Wilkerson et al. (2010) show a slight decline in 2006 at 162 Tg C. Figure 3 shows the annual column-integrated CO_2 emissions from aviation in GEOS-Chem for 2006, on a log scale.

Kim et al. (2005) partition the aviation fuel consumption (proportional to CO_2 emissions) into domestic and international components for eight regions of the world (roughly corresponding to the continents) for 2000–2004. Unlike international bunker fuels, domestic aviation fuel consumption is already included in national fossil fuel statistics and hence CO_2 inventories. Mean domestic aviation CO_2 emissions for 2000–2004, show that the North America region (which includes Central America and the Caribbean) has the highest level of domestic aviation CO_2 emitted (49.6 Tg C yr^{-1}), followed by Asia (16.1 Tg C yr^{-1}, excluding Russia and the Middle East) and Eastern Europe (12.3 Tg C yr^{-1}). The other regions combined account for a mean of 9.8 Tg C yr^{-1}. To avoid "double-counting" the CO_2 emissions from domestic aviation in both the aviation and our main fossil fuel source, we subtract them from the main fossil fuel inventory in the following way. Annual sums of national fossil fuel use for each of the eight regions are determined. By subtracting the regional domestic aviation CO_2 from this sum a new corrected sum is found, which is used to determine a scale factor for each region in each year. This scale factor (which is close to unity) is then applied to the fossil fuel emissions for each region so that the seasonality and the distribution within a region from the inventory are not changed, but CO_2 is conserved. With this approach, we maintain consistency with the assumed bunker fuel totals. For example in 2006, 189 Tg C came from international shipping and 65 Tg C from international aviation, within a fraction of a percent from the 255 Tg C emissions attributed to international bunker fuel.

Figure 4 shows the impact on atmospheric CO_2 from including shipping and aviation emissions in the model over multiple years. Differences are shown at the surface where ship emissions occur and at the model level near 11 km, which is the vertical level where aviation emissions are known to have the largest impact (Kim et al., 2007). This altitude is also close to the height of peak sensitivity for CO_2 retrieved from the thermal infrared satellite instruments AIRS (Chahine et al., 2005, 2008) and IASI (Crevoisier et al., 2009) and is therefore relevant for modeling work used in conjunction with those observations. In the first month shown in Fig. 4, the effects of shipping and aviation emissions are mainly local, with changes at the surface including both regions of increased CO_2 from the additional emissions and decreased CO_2 where the surface correction has been applied to avoid double-counting of domestic aviation emissions. Over time, the CO_2 perturbation spreads vertically and zonally, then mixes throughout the NH before it is transported to the Southern Hemisphere (SH). After 3 years there is a persistent latitudinal gradient in the

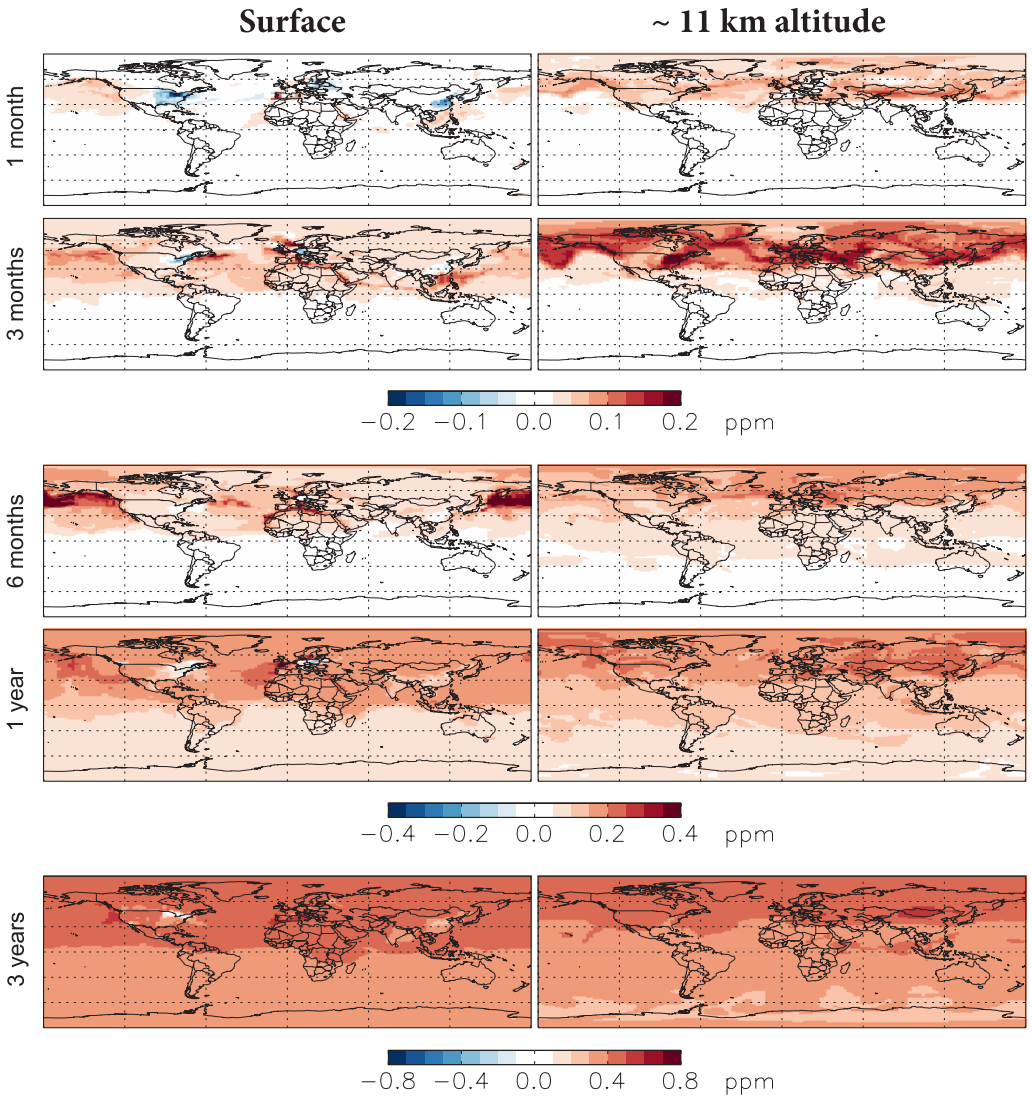

Fig. 4. Combined impact of shipping and aviation emissions on CO_2 at increments up to 3 years at the surface and at the model level near 11 km altitude where aviation emissions peak. The small negative CO_2 changes at the surface (which are most visible in the first month in the US and China) are a result of the correction to the land fossil fuel source to avoid counting emissions from domestic aviation in both inventories.

perturbation along with regions of nearly no increase where the adjustments to the land fossil fuel emissions were largest. The effect on the latitudinal gradient will be discussed quantitatively in Sect. 2.7.2.

2.7 Chemical production of CO_2 from the oxidation of atmospheric carbon species

2.7.1 Background and method

Carbon monoxide (CO), methane (CH_4) and non-methane volatile organic carbons (NMVOCs) are oxidized in the troposphere to produce CO_2 but very few attempts have been made to account for this chemical source in global CO_2 transport models or inverse modeling analyses. Early work on the subject was carried out first by Enting and Mansbridge (1991) with a 2-D model and later by Enting et al. (1995) with a 3-D model. This was followed by Baker (2001), Folberth et al. (2005) and Suntharalingam et al. (2005), while Ciais et al. (2008) considered the importance of the chemical contribution to the carbon balance of Europe. Chapter 7 of the Intergovernmental Panel on Climate Change (IPCC) Fourth Assessment Report (AR4, Denman et al., 2007) states the need for including the contribution from reduced carbon species in the total carbon budget or for the comparison of inversions with bottom-up estimates, but most recent CO_2 forward and inverse modeling work has ignored the issue or considered it negligible.

Fossil fuel emission inventories, such as from CDIAC, are based on CO_2 emission factors that include direct emissions of CO_2 from fossil fuels as well as the CO_2 that chemically forms elsewhere in the atmosphere from the emission of other carbon species (Marland and Rotty, 1984). Use of these inventories in a model results in the CO_2 contribution from oxidation occurring directly at the surface rather than at a later time and at some distant location in the atmosphere after considerable transport. Suntharalingam et al. (2005) quantified this error with model simulations using CO_2 production from oxidation distributed throughout the atmosphere and an appropriate quantity subtracted from the surface emissions based on the spatial distributions of precursor emissions from fossil fuels, biomass and biofuel burning, wetlands, ruminants, rice, termites and landfills, yielding a total of $1.10\,Pg\,C\,yr^{-1}$. The Suntharalingam et al. (2005) results have been directly applied offline by Jacobson et al. (2007b) in a joint global atmosphere-ocean inversion.

CO oxidation accounts for about 94% of the chemical production of CO_2 (Folberth et al., 2005) because CO is an intermediate for the oxidation of CH_4 and NMVOCs to CO_2 and CO_2 is the only significant product from CO oxidation. Therefore, we use the GEOS-Chem NO_x-O_x-hydrocarbon simulation to obtain monthly CO loss rates for the period 2004–2009 inclusive. These CO loss rates are essentially equal to the CO_2 production rates and are used in the model as a 3-D source inventory for the chemical production of CO_2.

Accounting for the surface correction requires accounting for emissions of all reactants that undergo oxidation to CO_2 that were already included in emission inventories, then appropriately subtracting that quantity. The surface correction discussed above is not necessary for inventories like GFED or the biofuel inventory, which explicitly account for CO_2, CO, CH_4 and NMVOC emissions using the emission factors of Andreae and Merlet (2001). The sum of fossil fuel contributions from these species is estimated at $0.30\,Pg\,C\,yr^{-1}$ for the 1988–1997 period (Suntharalingam et al., 2005; Duncan et al., 2007), for which mean global fossil fuel CO_2 emissions were $6.24\,Pg\,C\,yr^{-1}$ and the annual sum of national emissions was $6.13\,Pg\,C\,yr^{-1}$. The correction amounts to 4.89% of national emissions for 1988–1997, so we assume this constant percentage for contemporary values and proportionally scale down the spatially-distributed CDIAC emissions, assuming no regional variability in combustion completeness, although developed countries typically have stricter pollution controls and may have more complete combustion resulting in lower levels of CO, CH_4 and NMVOC emissions thus requiring a smaller correction factor.

Randerson et al. (2002) discuss the need for clarity in the definition of Net Ecosystem Production (NEP) and other quantities that are sometimes stated in terms of CO_2 and other times in terms of total carbon. Since they advocated for a definition including all carbon fluxes, non-CO_2 carbon emissions from CASA NEP (Olsen and Randerson, 2004) must be accounted for through a surface correction. To account for CH_4 from the biosphere we take the CH_4 source distribution from a GEOS-Chem CH_4 simulation for 2004, which includes monthly-averaged emissions from wetlands (bogs, swamps, tundra, etc.) and annually averaged emissions from livestock, landfills/waste, rice production and other natural sources (mainly termites). The combined annual sum of all biogenic methane sources is shown in Fig. 5 with the breakdown in Table 2. As in Duncan et al. (2007) and Suntharalingam et al. (2005), we assume a CH_4 to CO_2 conversion efficiency of unity. Other biogenics are accounted for using the spatial distribution of isoprene and monoterpenes from a 2004 GEOS-Chem simulation that was run using emission factors from the MEGAN inventory (Guenther et al., 2006, 2007). This yielded annual biospheric emissions of 351 Tg C of isoprene and 132 Tg C of monoterpenes. Figure 5 shows that the most intense biospheric emissions of isoprene and monoterpenes came from the Amazon, equatorial Africa, Indonesia and the south-eastern United States. Unlike methane, the conversion efficiency of these species to CO is only about 0.20 (Duncan

Table 2. Global annual component values for the surface correction that accompanies CO_2 chemical production from the oxidation of reduced carbon. The total surface correction and total chemical production are also shown.

Reduced Carbon Source of CO_2	Annual Contribution ($Pg\,C\,yr^{-1}$)	
	for 1988–1997 from Suntharalingam et al. (2005)	for 2006 from this work
Fossil Fuel Burning [a]	0.30	0.383
Biomass Burning[a]	0.256	0[b]
Biofuel Burning[a]	0.08	0[b]
Total Biospheric CH_4	0.304	0.281
Wetlands	0.14	0.120
Ruminants	0.062	0.080
Rice	0.044	0.025
Termites	0.019	0.009
Landfills	0.039	0.047
Total Biospheric NMVOCs	0.16	0.161
TOTAL Surface Correction	1.10	0.825[c]
TOTAL Chemical Production	1.10	1.045[c]

[a] Consists of the sum of CO, CH_4 and NMVOCs.

[b] Specific carbon gases are individually accounted for in GFEDv2 and the biofuel inventory.

[c] CO_2 chemical production and the surface correction are not balanced in our approach (as they were in Suntharalingam et al., 2005) due to a different treatment of biomass and biofuel emissions.

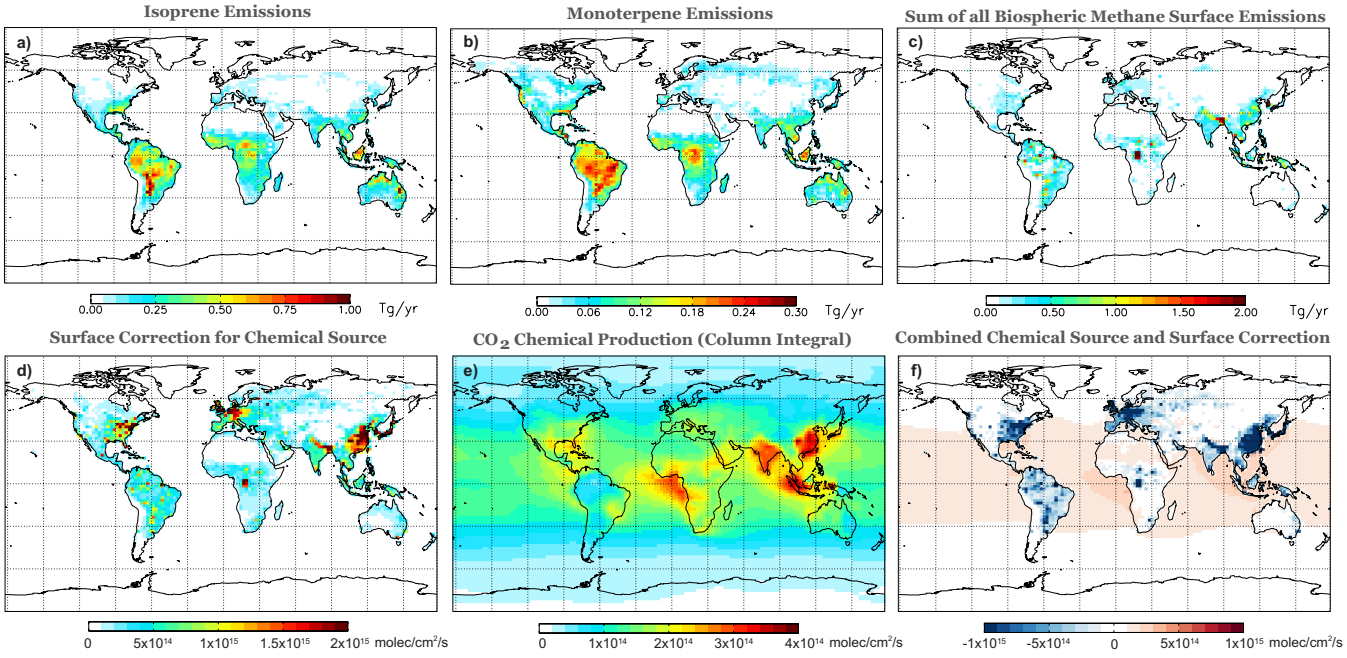

Fig. 5. Key components of the 3D chemical source and surface correction for 2006. **(a)** Distribution of isoprene emissions from a GEOSChem full chemistry simulation using MEGAN. **(b)** Distribution of monoterpene emissions from a GEOS-Chem full chemistry simulation using MEGAN. **(c)** Distribution of total biospheric CH_4 emissions (wetlands, ruminants, landfills, rice, termites) from a GEOS-Chem CH_4 simulation. **(d)** Surface correction due to all biogenic and fossil fuel emissions to avoid double-counting emission of CO_2 precursor species (CO, CH_4 and NMVOCs) shown on a log scale. **(e)** Column sum of CO_2 production rates based directly on CO loss rates from a GEOS-Chem NO_x-O_x-hydrocarbon (full chemistry) simulation. **(f)** Column sum of panels **(d)** and **(e)**.

et al., 2007) but we instead apply a conversion factor of 0.333 to scale the isoprene and monoterpene distribution to account for all other NMVOCs, thus giving an annual total of 160 Tg C yr^{-1} as in Suntharalingam et al. (2005), which was based on Duncan et al. (2007). The total annual CO_2 production and the associated surface correction for 2006 are given in Table 2 along with values from Suntharalingam et al. (2005). Our surface corrections are smaller than those of Suntharalingam et al. (2005) and not balanced with our CO_2 chemical production, since we have not adjusted surface emissions for chemical production related to biomass and biofuel burning inventories since they already use separate emission factors for each individual species (van der Werf et al., 2006; Yevich and Logan, 2003; Andreae and Merlet, 2001).

Figure 6 displays the vertical, latitudinal and monthly variability in CO_2 chemical production for selected months in 2006. Peak production typically occurs from the surface to about 4 km in the NH tropics, however in September to November 2006, intense CO_2 production occurred in the SH, likely related to Indonesian biomass burning. This can be confirmed by the spatial patterns in Fig. 7, which shows the monthly chemical production of CO_2 at model level 22, near 5 km altitude. This altitude was selected for comparison since it is the altitude of peak sensitivity for CO_2 measurements by the Tropospheric Emission Spectrometer

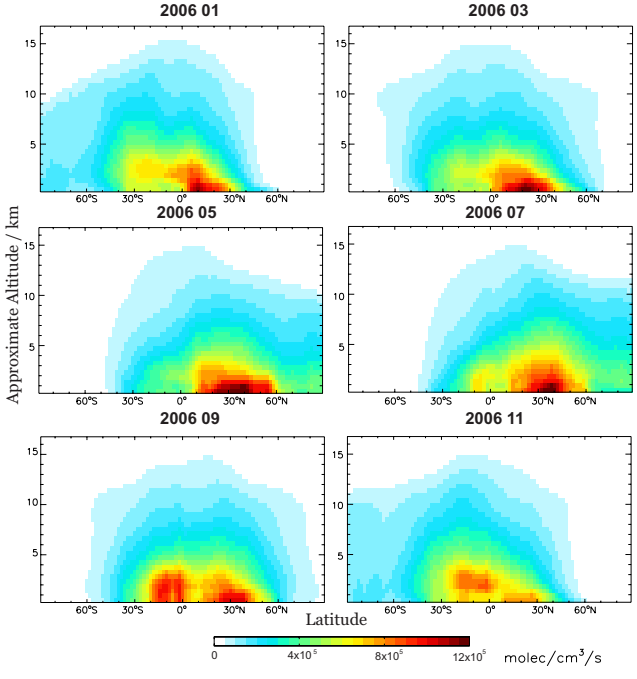

Fig. 6. Monthly vertical and latitudinal distribution of CO_2 chemical production for 2006. Altitudes are only approximate because they are based on conversion from model hybrid sigma levels.

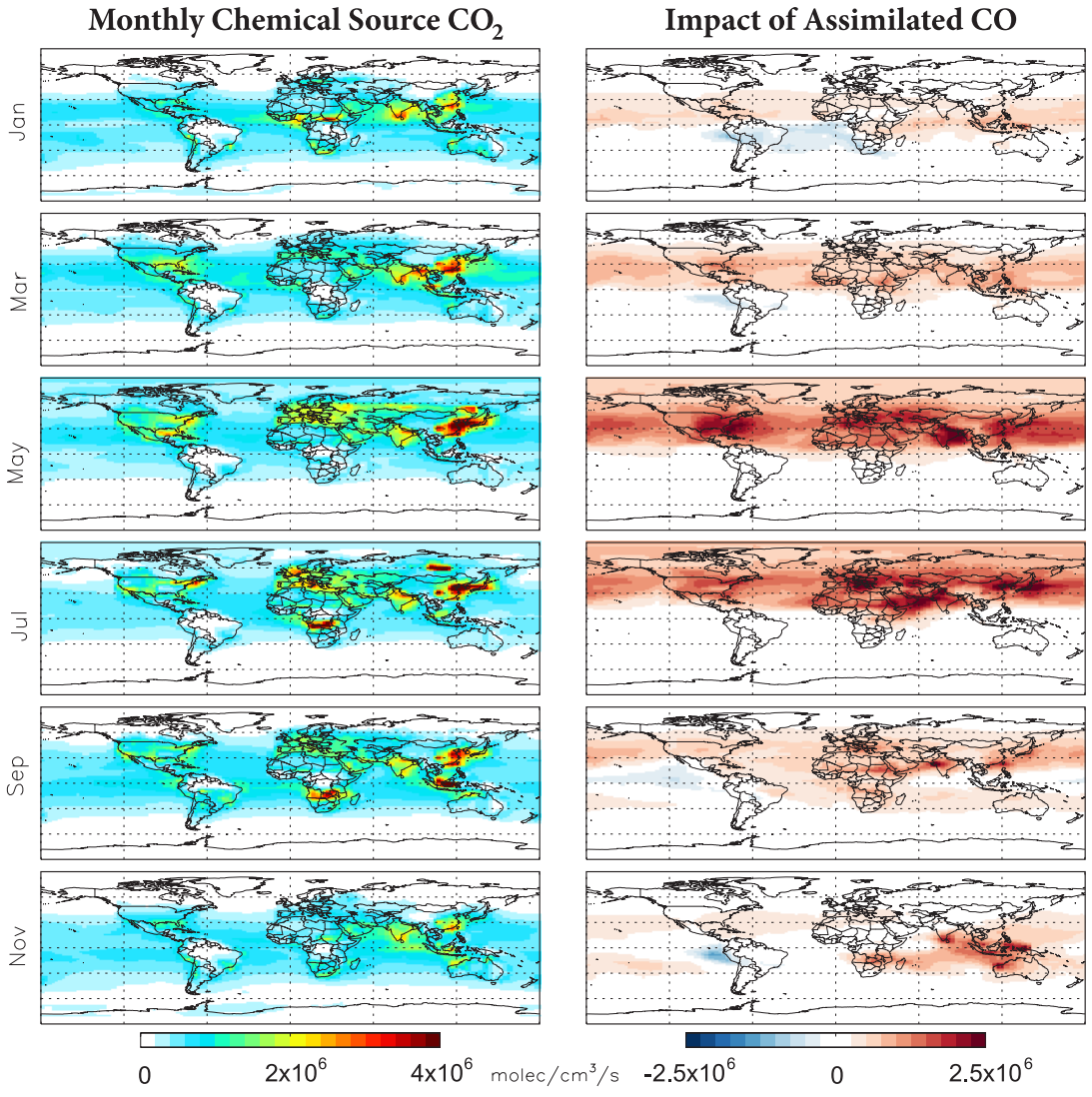

Fig. 7. Monthly CO_2 chemical source production rates in 2006 within the model level nearest to 5 km (left). The impact of using assimilated CO relative to the purely modeled chemical production of CO_2 for the same model level (right).

(TES) (Kulawik et al., 2010), which are beginning to be used for assimilation with GEOS-Chem CO_2 simulations (Nassar et al., 2010). In both Figs. 6 and 7, chemical production of CO_2 exhibits clear local, latitudinal and seasonal variability which should impact inverse modeling. The most intense chemical production is mainly localized over China but is occasionally seen in other regions, most likely related to biomass burning, such as over Siberia in July, Indonesia from August to November and southern Australia in December (not shown). Although the CO_2 chemical production is mainly bounded by 60° S–60° N, significant CO_2 production is observed in the Arctic and the Antarctic during their respective summers. Interestingly, no biomass burning signature is seen over the Amazon, which is a local minimum in CO_2 production for most months at this level, thus indicating that conversion of CO to CO_2 is dependent on multiple chemical and dynamical factors and not just the quantity of CO present. The annual column average CO_2 chemical production and the combined production plus surface correction (sometimes referred to as the chemical pump) are shown in Fig. 5. The chemical pump mostly shows a decrease over land areas and an increase over oceans from ∼ 30° S–35° N, which will have an impact when applying the model simulation to inverse modeling of terrestrial surface fluxes.

2.7.2 Impact of the chemical pump on atmospheric CO_2

The impact of the chemical pump is shown in Fig. 8 at the surface and at the model level near 5 km, for time intervals of up to 3 years. After one month, we see locally decreased CO_2 at the surface in the NH, with almost no effects at

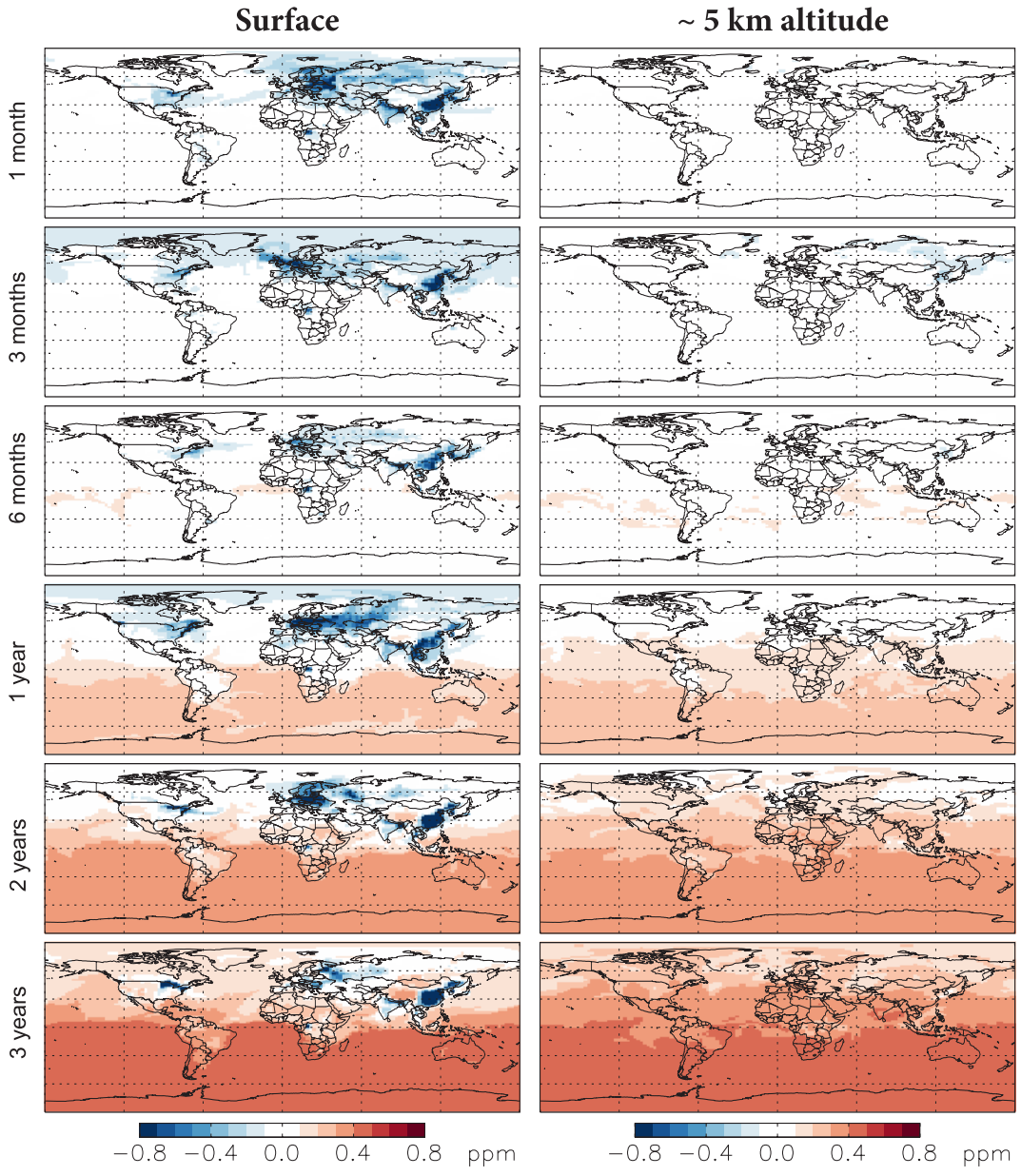

Fig. 8. Difference maps showing the impact of CO_2 chemical production and the surface correction (determined as: chemical source simulation – no chemical source simulation) at the surface and at the model level near 5 km for increments up to 3 years. The negative anomalies at the surface are a result of the surface correction.

5 km. After 3 months, we see regions of decreased CO_2 in the NH at the surface, with a similar pattern at 5 km albeit somewhat weaker. Although a negative perturbation from the chemical source persists at the surface from 6 months to 3 years, at 5 km altitude the perturbation is positive globally beyond about 6 months with a strong latitudinal gradient. After 3 full years the perturbation at 5 km slightly exceeds the perturbation at the surface for high southern latitudes. The zonally-averaged impacts of the chemical source and emissions from shipping and aviation are shown in Fig. 9 for both the surface and the model level nearest to 5 km. This indicates a decrease of ~ 0.25 ppm in the gradient between Mauna Loa (19.54° N) and the South Pole after one year as a result of the chemical source. After 4 complete years, the zonal impact of the chemical source in the SH is $\sim$ 0.60 ppm while for NH midlatitudes it ranges from $\sim 0.15-$ 0.25 ppm. The zonal impact from shipping and aviation in Fig. 9, partially offsets the impact of the chemical source on the latitudinal gradient. By the end of the fourth year, the combined impact of shipping and aviation emissions

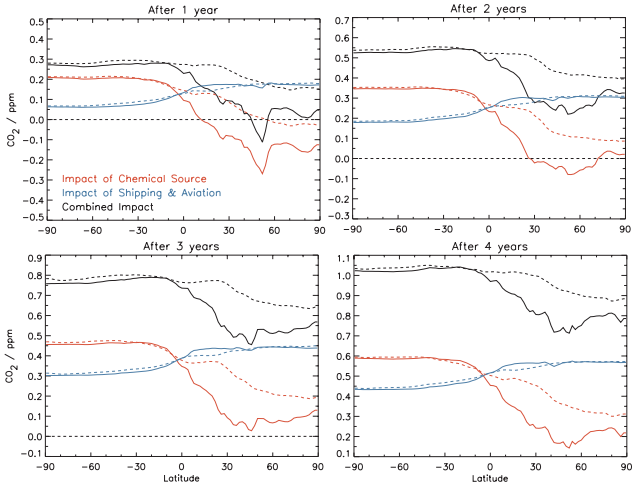

Fig. 9. Cumulative impact of shipping, aviation and the chemical source as a function of latitude. The impacts were determined by subtracting zonally-averaged CO_2 from runs with and without shipping and aviation emissions, and runs with and without the chemical source. The solid lines show the impacts at the surface and the dotted lines show the impacts at the model level near 5 km. Runs began with a uniform initialization of 375.0 ppm on 1 January 2004.

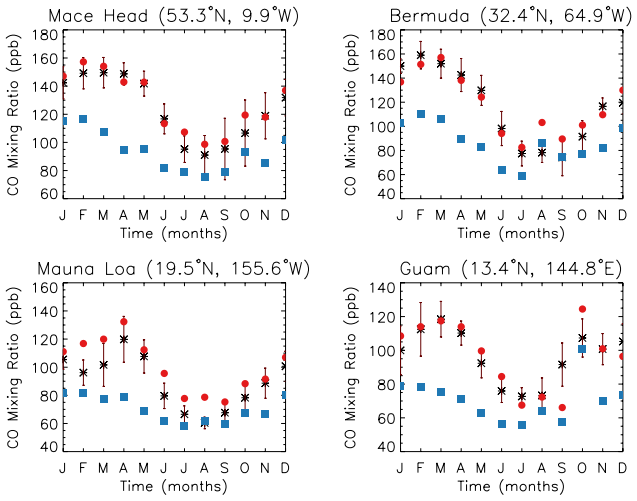

Fig. 10. Monthly-averaged model CO (blue squares) and the model with assimilated TES CO (red circles) compared with CO surface measurements (black asterisks) in 2006. Error bars on the measurements denote the one standard deviation variability in CO at that station for the given month during the period of 1996–2006.

with CO_2 chemical production is ~ 1.0 ppm in the SH, and somewhat less in the NH with a minimum of ~ 0.70 ppm around 40–50° N. It should be noted that the simulation maintains a persistent change in gradient even after much inter-hemispheric mixing has occurred. While shipping and aviation increase the global CO_2 latitudinal gradient by just over 0.1 ppm, the inclusion of CO_2 chemical production (and the surface correction) decreases the latitudinal gradient by about 0.40 ppm with a complex spatial structure generally resulting in decreased CO_2 over land and increased CO_2 over the oceans.

The global offset in CO_2 mixing ratios which results from inclusion of the chemical source specifically relates to the additional CO_2 in the model system due to the imbalance between the chemical source and the surface correction (Table 2), associated with reduced carbon emissions from biomass and biofuel combustion. We do not correct for them here as our surface emissions from biomass burning and biofuel combustion (derived from GFED and Yevich and Logan, 2003) include only direct emissions of CO_2.

2.7.3 Assimilated CO for determination of CO_2 production rates

A major limitation in using the O_x-NO_x-hydrocarbon model simulation to estimate the chemical source of CO_2 is that bottom-up CO inventories are highly uncertain. For example, Kopacz et al. (2010) conducted an inversion analysis of CO observations from four different satellite instruments and found that the CO emission inventory in GEOS-Chem significantly underestimated wintertime CO emission. Inferred emissions from North America and Europe were 50% larger in winter than the specified bottom-up emissions in the model, whereas inferred emission estimates from Asia were 100% greater in winter. Kopacz et al. (2010) attributed this discrepancy to an underestimate of emissions from vehicle engine cold starts and residential heating in the bottom-up inventory. These biases in the bottom-up inventory will result in an underestimate of the CO_2 production rate calculated from the model. An alternative approach is to assimilate observations of atmospheric CO to obtain an improved description of the CO distribution in the model and, thus, a more accurate estimate of CO_2 production rates.

Parrington et al. (2008) used a sequential sub-optimal Kalman filter to assimilate TES observations of ozone and CO into the GEOS-Chem O_x-NO_x-hydrocarbon simulation. We have extended the Parrington et al. (2008) study to assimilate TES CO data for 2006 into the current version of GEOS-Chem. We focus on 2006 for the assimilation since TES data only became available in fall of 2004 and the TES measurements in 2005 had low sensitivity to tropospheric CO. TES CO sensitivity increased significantly after warm-up of the instrument's optical bench in December 2005. Assimilation of TES CO significantly increases the CO abundance in the model, consistent with the results of Kopacz et al. (2010), and improves the agreement with CO surface measurements from the NOAA-ESRL-GMD network (http://www.esrl.noaa.gov/gmd/ccgg/trends/#global). Figure 10 compares monthly-averaged model and assimilated CO with measurements at four of these stations.

The right panels in Fig. 7 show the impact of basing our CO_2 production on assimilated TES CO observations for 2006. The CO_2 production rates are weakly enhanced between $\sim 0-40^\circ$ N from January to March. In January the globally averaged production rate is about 5% larger with the assimilation, whereas in March it is 13% greater. There are small reductions in the CO_2 production rates over the Amazon and across the Atlantic to southern Africa in January. The largest differences in CO_2 production rates are obtained between $0-40^\circ$ N during May to June, when the assimilation enhances the globally-averaged CO_2 production by as much as 24%. The assimilation results in an increase in the global annual CO_2 production rate from 1.045 Pg C yr^{-1} to 1.181 Pg C yr^{-1}. After a 1-year simulation (2006), the run with assimilated CO produced CO_2 that was ~ 0.08 ppm higher than our standard chemical production run near 5 km over much of the NH and a localized perturbation of 0.85 ppm at this altitude over equatorial Africa. To our knowledge, this represents the first satellite-derived estimate of the chemical source of CO_2. We are exploring further the use of the assimilation of TES CO data in our inversion analysis of the TES CO_2 data.

3 GEOS-Chem CO_2 simulations and comparisons

In this section, we will evaluate GEOS-Chem CO_2 simulations that have used the fluxes described in the previous section. The primary simulation was carried out using GEOS-5 meteorological fields at 2° latitude $\times$ 2.5° longitude resolution, with 47 vertical hybrid-sigma levels up to 0.01 hPa. Since CO_2 has a long atmospheric lifetime, initial concentrations strongly impact model results. The total global average CO_2 in the model atmosphere at the start of the run will have a much larger impact than specific features of the CO_2 distribution. For this work, we begin with a uniform global distribution of 375 ppm for 1 January 2004 and rely on the model transport, sources and sinks to develop spatial patterns of CO_2. According to the NOAA-ESRL-GMD website (provided in Sect. 2.7.3), the global marine surface annual mean CO_2 in 2003 was 374.93 ppm, with monthly means of 376.31 ppm in December 2003 and 376.97 ppm in January 2004. The total tropospheric mean CO_2 for 1 January 2004 is related to these values but also dependent on values over land which are highly variable but tend to be slightly higher than marine values in January, as well as the vertical profile of CO_2, which generally decreases with height in the NH and increases slightly with height in the SH. These facts make approximating mean tropospheric CO_2 difficult, but suggest that 375 ppm for 1 January 2004 is a reasonable starting point for a spin-up and subsequent simulation. In the following section, we examine model results from the aforementioned run.

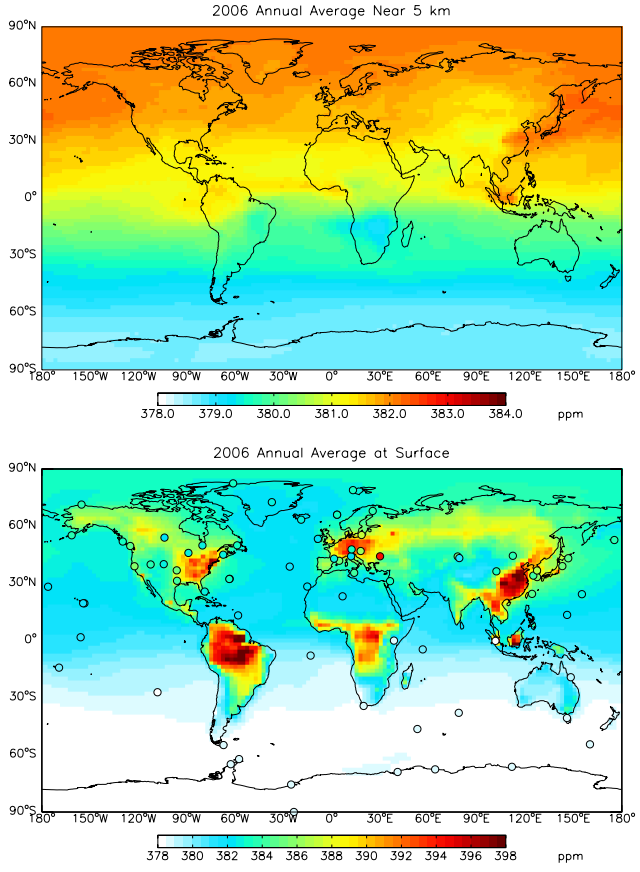

Fig. 11. Annually-averaged 2006 model CO_2 from a run with emissions from shipping, aviation and the chemical source. The upper panel shows CO_2 at the model level near 5 km and the lower panel shows model CO_2 at the surface level compared with 74 GLOBALVIEW-CO_2 stations on the same color scale (colored circles).

3.1 Spatial and temporal comparisons with GLOBALVIEW-CO_2

Figure 11 shows the annually averaged GEOS-Chem CO_2 concentration for 2006 at the surface and around 5 km, from a run with emissions from shipping, aviation, the chemical source and other fluxes. CO_2 values are generally higher in the NH with a gradual pole-to-pole gradient at both altitudes. This gradient is mainly a result of the predominant emission of fossil fuel CO_2 occurring in the NH and is roughly consistent with the expected gradient based on 2006 emission values (Taylor and Orr, 2000; Keeling et al., 2005), and is discussed more quantitatively later. The model level near 5 km clearly shows a smaller range of values than at the surface as well as a reduced distinction between CO_2 over land and ocean. Overall, the difference between minimum and maximum values in annually-averaged surface CO_2 shown in Fig. 11 is only ~ 25 ppm or $\sim$6%, which is much smaller than those for tropospheric trace gases with shorter lifetimes such as CO, O_3 (i.e. Nassar et al., 2009) or CH_4.

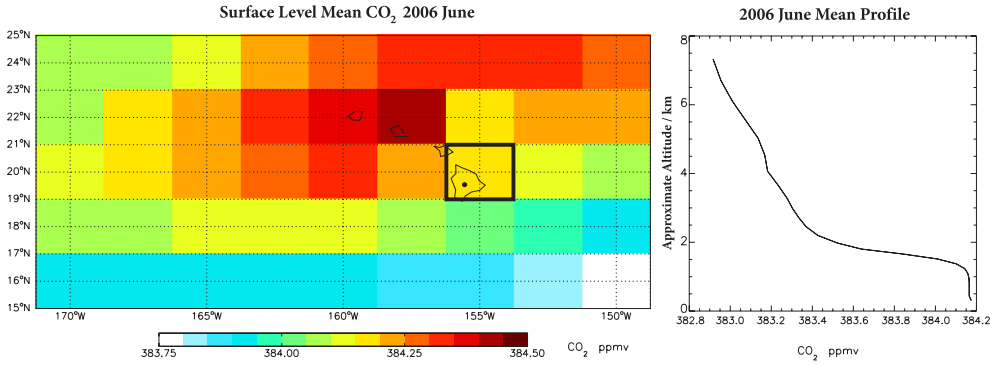

Fig. 12. GEOS-Chem mean surface level CO_2 for 2006 June for the Hawaiian Islands region (left). The CO_2 profile for the gridbox containing Mauna Loa (right) corresponds to the area outlined in black in the left panel. Altitude is only approximate for the profile because it is based on a conversion from model hybrid sigma levels which requires assuming a surface pressure that will vary throughout the gridbox (222 km × 261 km) from sea level to about 4.2 km altitude. The location of the Mauna Loa observatory is shown by the black dot.

It should be noted that this range is somewhat specific to a resolution of 2° × 2.5° and a finer resolution (or true point measurements) would lead to a slightly larger range.

Figure 11 compares the model simulations with 74 GLOBALVIEW-CO_2 (GLOBALVIEW, 2009) sites (listed in Table 3), exhibiting good agreement for large-scale features of the model in the third year of a completely unconstrained simulation. The simulation represents the north-south CO_2 gradient reasonably well, although some differences are noticeable at high southern latitudes (less than 0.5 ppm) and will be discussed in detail later. Agreement at marine and coastal sites is better than that at inland sites (for example in Europe), which can be affected by strong inland sources and sinks.

Representativeness errors due to finite resolution are a serious limitation of current CO_2 models and complicate these comparisons. This issue has been investigated by Gerbig et al. (2003a, b) for in situ observation of CO_2 and by Pillai et al. (2010) for satellite observations. Figure 12 illustrates this problem for Mauna Loa, by displaying the horizontal surface variability around Hawaii and the vertical profile of the Mauna Loa gridbox. Although we can have very accurate in situ point measurements or flask measurements, comparing these to the model is a challenge because of representativeness. In the horizontal direction, the gridbox with which we compare is 222 km × 261 km, encompassing the big island of Hawaii, a portion of a smaller island (Maui) and much of the ocean. True horizontal variability in the CO_2 mixing ratio, which the point measurement only samples, is averaged over the entire gridbox in the model, which can lead to an apparent discrepancy although both values could be accurate. Vertical representativeness errors are even more of a challenge. Mauna Loa measurements sample air at 3.4 km up the peak of the 4.2 km mountain, but because of the topography within this gridbox, the lowest model level spans 0–4.2 km altitude while a single surface pressure must be used in determining the model hybrid sigma level. The mean surface pressure of the gridbox will be ocean-like since ∼75% of the box is ocean, yet we can see that over this vertical range, the CO_2 profile exhibits a drop of about 1.0 ppm. Many GLOBALVIEW sites are situated on islands or coastal areas in an attempt to sample background CO_2 levels, which is a logical strategy to minimize representativeness errors due to sources and sinks, but it should be noted that this can inadvertently amplify errors related to elevation.

To evaluate the model seasonal cycle, we make timeseries comparisons between point measurements at a number of GLOBALVIEW locations. In Fig. 13, timeseries comparisons are made between GLOBALVIEW and a multi-year simulation with shipping, aviation, the chemical source and other fluxes for the period of 1 January 2004 to 31 December 2008. A 7-day moving average (based on 4 points in the diurnal cycle spaced 6-h apart) has been applied to the modeled data, while the GLOBALVIEW consists of ∼7.6-day averages, with a 40-day low-pass filter applied to residuals (Masarie and Tans, 1995). More variability is evident in the model timeseries than the GLOBALVIEW timeseries, which appears smoother as a result of the low-pass filtering. We do not apply the same filtering approach to our data since this variability on short time scales in the model could be of interest for certain applications, but should theoretically average out over time.

Aside from the fine scale features of the model CO_2 timeseries, the model represents the seasonal variability at each station reasonably well. The characteristic near-sinusoidal seasonal cycle is largest in the mid- to high-latitudes of the NH over land (such as Fraserdale) consistent with NH vegetation absorbing CO_2 in the boreal growing season and the release of CO_2 by vegetation at the end of the growing season (Keeling, 1960). This pattern is predominantly driven by terrestrial fluxes from CASA, while much smaller contributions to the seasonal cycle include fossil fuel burning, biomass burning, ocean exchange and

Table 3. GLOBALVIEW-CO_2 stations used for comparisons with GEOS-Chem in this work (GLOBALVIEW, 2009).

Station	Abbreviation	Latitude	Longitude	Elevation (m)	Date Range	Fig. 14[b]
Alert, Nunavut	alt_06C0	82.45	–62.51	210	Jun 1987–Feb 2009	*
Amsterdam Island, France	ams_11C0	–37.95	77.53	150	Jan 1981–Dec 2005	
Argyle, Maine	amt012_01C3	45.03	–68.68	50 + 12[a]	Sep 2003–Dec 2008	
Ascension Island, UK	asc_01D0	–7.92	–14.42	54	Aug 1979–Feb 2009	*
Assekrem, Algeria	ask_01D0	23.18	5.42	2728	Sep 1995–Feb 2009	
Terceira Island, Azores	azr_01D0	38.77	–27.38	40	Dec 1979–Feb 2009	*
Baltic Sea, Poland	bal_01D1	55.35	17.22	3	Sep 1992–Feb 2009	
Begur, Spain	bgu_11D0	41.83	3.33	30	Feb 2000–Dec 2007	
Bukit Kototabang, Indonesia	bkt_01D0	–0.20	100.32	864	Jan 2004–Feb 2009	
St. David's Head, Bermuda	bme_01D0	32.37	–64.65	30	Feb 1989–Oct 2008	
Tudor Hill, Bermuda	bmw_01D0	32.27	–64.88	30	May 1989–Feb 2009	
Barrow, Alaska	brw_01C0	71.32	–156.61	11	Jul 1973–Dec 2008	*
Black Sea, Romania	bsc_01D0	44.17	28.68	3	Mar 1995–Feb 2009	
Cold Bay, Alaska	cba_01D0	55.21	–162.72	21	Oct 1978–Dec 2007	*
Candle Lake, Saskatchewan	cdl030_06C3	53.99	–105.12	600 + 30[a]	Aug 2002–Feb 2009	
Cape Ferguson, Australia	cfa_02D0	–19.28	147.06	2	Jun 1991–Jan 2009	
Cape Grim, Tasmania	cgo_02D0	–40.68	144.69	94 + 70[a]	Apr 1984–Feb 2009	
Christmas Island, Kiribati	chr_01D0	1.70	–157.17	3	Mar 1984–Feb 2009	*
Mt. Cimone, Italy	cmn_17C0	44.18	10.70	2165	Mar 1979–Dec 2006	
Cape Ochi-Ishi, Japan	coi_20C0	43.15	145.50	100	Aug 1995–Dec 2007	
Cape Point, South Africa	cpt_36C0	–34.35	18.49	230 + 30[a]	Sep 1993–Dec 2008	
Crozet Island, France	crz_01D0	–46.45	51.85	120	Mar 1991–Feb 2009	*
Cape St. James, BC	csj_06D0	51.93	–131.02	89	May 1979–Jul 1991	
Casey, Antarctica	cya_02D0	–66.28	110.52	51	Jun 1997–Dec 2008	
Easter Island, Chile	eic_01D0	–27.15	–109.45	50	Jan 1994–Feb 2009	*
Estevan Point, BC	esp_06D0	49.58	–126.37	7	Jun 1992–Feb 2009	
Fraserdale, Ontario	frd040_06C3	49.88	–81.57	210 + 40[a]	Feb 1990–Feb 2009	
Mariana Islands, Guam	gmi_01D0	13.43	144.78	1	Mar 1979–Feb 2009	*
Gosan, Korea	gsn_24D0	33.28	126.15	72	Oct 1990–Feb 2009	
Hateruma Island, Japan	hat_20C0	24.05	123.80	47	Oct 1993–Dec 2007	
Halley, Antarctica	hba_01D0	–75.58	–26.50	30	Jan 1983–Dec 2008	*
Hohenpeissenberg, Germany	hpb_01D0	47.80	11.01	985	Apr 2006–Feb 2009	
Hegyhatsal, Hungary	hun010_35C3	46.95	16.65	248 + 10[a]	Sep 1994–Dec 2007	
Storhofdi, Iceland	ice_01D0	63.40	–20.29	118	Oct 1992–Feb 2009	
Tenerife, Canary Islands	izo_27C0	28.31	–16.50	2360	Jun 1984–Feb 2009	
Jubany, Antarctic Peninsula	jbn_29C0	–62.23	–58.82	15	Mar 1994–Dec 2008	*
Key Biscayne, Florida	key_01D0	25.67	–80.16	3	Dec 1972–Feb 2009	
Cape Kumukahi, Hawaii	kum_01D0	19.52	–154.82	3	Mar 1976–Feb 2009	
Sary Taukum, Kazakhstan	kzd_01D0	44.08	76.87	601	Oct 1997–Feb 2009	
Plateau Assy, Kazakhstan	kzm_01D0	43.25	77.88	2519	Oct 1997–Feb 2009	
Park Falls, Wisconsin	lef011_01C3	45.95	–90.27	472 + 11[a]	Jul 2003–Dec 2008	
Lampedusa, Italy	lmp_28D0	35.52	12.62	45	Jan 1996–Dec 2005	
Mawson, Antarctica	maa_02D0	–67.62	62.87	32	Nov 1990–Jan 2009	
Mace Head, Ireland	mhdrbc_11C0	53.33	–9.90	25	Jul 1992–May 2008	
Sand Island, Midway	mid_01D0	28.21	–177.38	3	May 1985–Feb 2009	*
Mount Kenya, Kenya	mkn_01D0	–0.05	37.30	3897	Dec 2003–Feb 2009	
Mauna Loa, Hawaii	mlo_01C0	19.54	–155.58	3397	May 1974–Dec 2008	*
Minamitorishima, Japan	mnm_19C0	24.30	153.97	8	Feb 1993–Dec 2008	
Macquarie Island, Australia	mqa_02D0	–54.48	158.97	12	Feb 1991–Jan 2009	*
Niwot Ridge, Colorado	nwr_01D0	40.05	–105.58	3523 + 5[a]	Jan 1968–Feb 2009	
Pallas-Sammaltunturi, Finland	pal_01D0	67.97	24.12	560	Dec 2001–Feb 2009	
Pic du Midi, France	pdm_11D0	42.93	0.13	2877	Jun 2001–Oct 2007	
Palmer, Antarctica	psa_01D0	–64.92	–64.00	10	Jan 1978–Feb 2009	
Point Arena, California	pta_01D0	38.95	–123.74	17	Jan 1999–Feb 2009	
Ragged Point, Barbados	rpb_01D0	13.17	–59.43	45	Nov 1987–Feb 2009	

Table 3. Continued.

Station	Abbreviation	Latitude	Longitude	Elevation (m)	Date Range	Fig. 14[b]
Ryori, Japan	ryo_19C0	39.03	141.83	260	Jan 1987–Dec 2008	
Sable Island, Nova Scotia	sbl_06C0	49.93	–60.02	5	Aug 1992–Feb 2009	
Mahe Island, Seychelles	sey_01D0	–4.67	55.17	3	Jan 1980–Feb 2009	
Southern Great Plains, Oklahoma	sgp374_01D0	36.80	–97.50	314	Apr 2002–Feb 2009	
Shemya Island, Alaska	shm_01D0	52.72	174.10	40	Sep 1985–Feb 2009	*
Tutuila, American Samoa	smo_01D0	–14.25	–170.56	42	Aug 1973–Feb 2009	*
South Pole, Antarctica	spo_01C0	–89.98	–24.80	2810	Jul 1975–Jan 2009	*
Ocean Station M, Norway	stm_01D0	66.00	2.00	5	Mar 1981–Feb 2009	
Summit, Greenland	sum_01D0	72.58	–38.48	3238	Jun 1997–Feb 2009	
Syowa, Antarctica	syo_01D0	–69.00	39.58	11	Feb 1986–Jan 2009	
Tae-ahn Peninsula, Korea	tap_01D0	36.73	126.13	20	Nov 1990–Feb 2009	
Tiera Del Fuego, Argentina	tdf_01D0	–54.87	–68.48	20	Sep 1994–Feb 2009	*
Wendover, Utah	uta_01D0	39.90	–113.72	1320	May 1993–Feb 2009	
Ulann Uul, Mongolia	uum_01D0	44.45	111.10	914	Jan 1992–Feb 2009	
Sede Boker, Israel	wis_01D0	31.13	34.88	400	Nov 1995–Feb 2009	
Moody, Texas	wkt030_01C3	31.32	–97.33	251 + 30[a]	Feb 2004–Dec 2008	
Mt. Waliguan, China	wlg_33C0	36.29	100.90	3810	Nov 1994–Nov 2008	
Yonagunijima, Japan	yon_19C0	24.47	123.02	30	Jan 1997–Dec 2008	
Ny-Alesund, Svalbard	zep_01D0	78.90	11.88	475	Feb 1994–Feb 2009	

[a] The first number is the land elevation and the second is the tower height.

[b] Asterisks (*) indicate that the station was used in the zonal gradient comparison (Fig. 14).

the chemical source. (The magnitude of the seasonal impact from fossil fuel emissions is quantified and discussed earlier). The seasonal cycle amplitude typically decreases moving southward, since the SH has less midlatitude vegetation to seasonally absorb and release CO_2. The least seasonal variability is evident at Antarctic locations and in particular the South Pole, farthest from sources and sinks. There are a few exceptions to this generally good agreement, with the largest discrepancy at the Indonesian station Bukit Kototabang (0.20° S, 100.32° E, 864 m), for which the raw flask data and GLOBALVIEW-CO_2 data have values lower than the South Pole station. The discrepancy is attributed to measurement sampling during the local afternoon when there is a significant drawdown of CO_2 by the Sumatran forests (P. Tans, personal communication, 2010). GLOBALVIEW-CO_2, which was originally designed for background CO_2 does not account for effects of the diurnal cycle in its interpolation to an even temporal grid.

Since the initialization of the model run began on 1 January 2004 with a uniform CO_2 distribution, the start of the timeseries have low biases at NH high latitudes (Alert, Summit, Barrow) and smaller high biases at SH high latitudes (South Pole, Cape Grim, Macquarie Island). For Mauna Loa, much of the tropics and many SH stations, the uniform global value is already a close approximation. After less than 6 months of the model spin-up, realistic features develop including better agreement at the higher latitudes as a result of the various drivers of the rectifier effect, hence our timeseries figure begins at the start of 2005.

The model exhibits a slight high drift over time, with the departure from GLOBALVIEW mainly becoming evident in 2007. Some drift as observed here is expected since we are running with an annual terrestrial exchange climatology (based on the 1991–2000 period) and ocean exchange that are not increasing in conjunction with increasing fossil fuel CO_2 emissions. A strong body of evidence indicates that as emissions increase, Earth's natural sinks are taking up greater amounts of CO_2 since only very subtle trends are observed in the airborne fraction (Gloor et al., 2010). For use of the model simulations in the context of data assimilation or inverse modeling, observational data will constrain the drift or minimize the error in a posteriori fluxes as necessary, but doing this correctly requires precise observations and sufficient global coverage.

Figure 14 illustrates the latitudinal gradient obtained from our simulations with and without the chemical source. Here we see that the chemical source gives persistently better agreement with GLOBALVIEW-CO_2 in the SH, where the run without the chemical source is persistently lower than GLOBALVIEW-CO_2. For the NH, the run with the chemical source is superior for two out of three years, but is positively biased in 2007. Since the CO_2 chemical source is indeed a real contributor to atmospheric CO_2, the fact that the drift is greater when it is included highlights the fact that sinks such as annual terrestrial uptake are likely increasing at an even greater rate than we might diagnose by simply examining the model data mis-match in the no-chemistry runs. It is very likely that by 2007, terrestrial exchange is much stronger

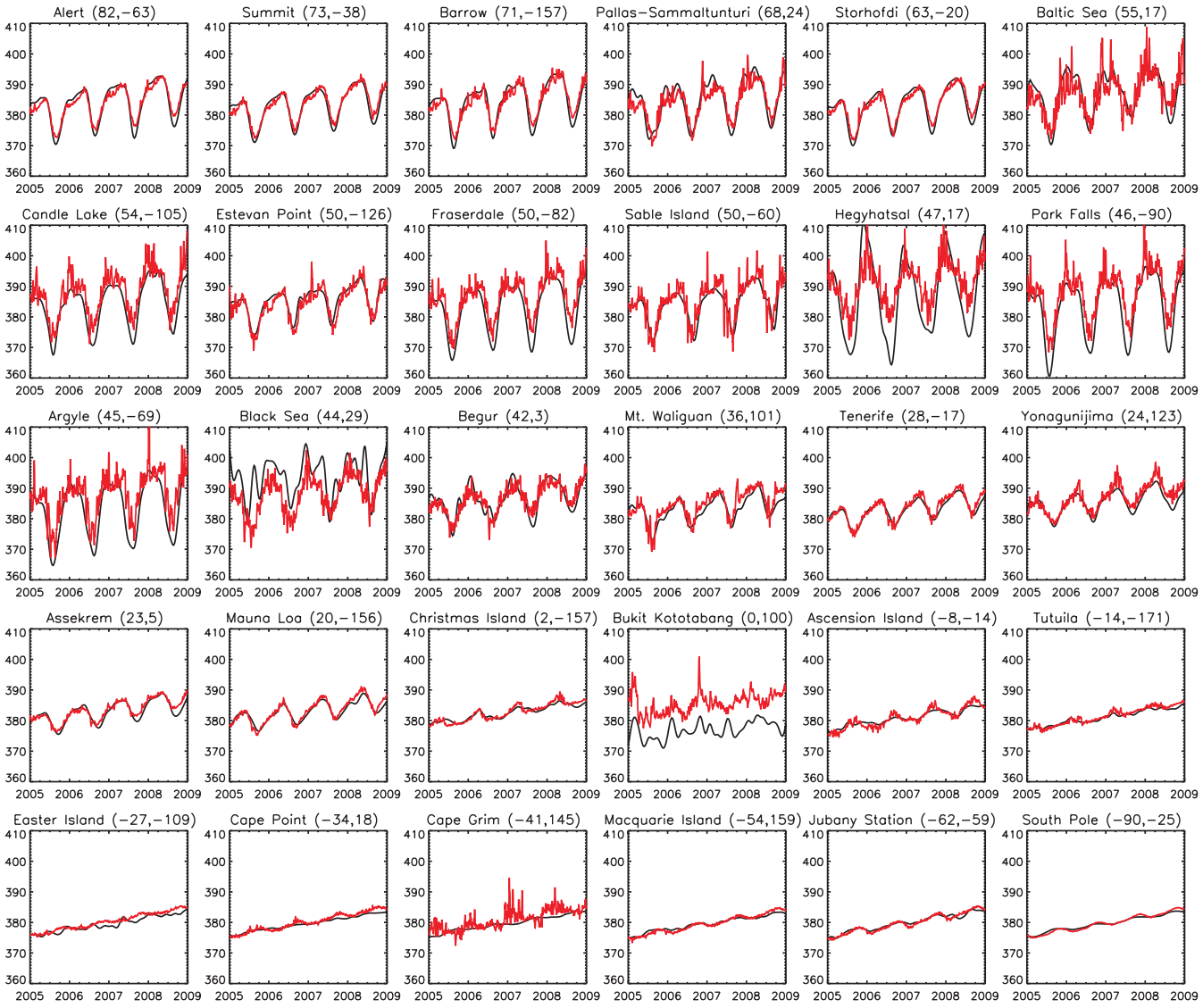

Fig. 13. 7-day averaged GEOS-Chem CO_2 with the chemical source on (red) compared with GLOBALVIEW-CO_2 smoothed ∼ 7.6-day average (black) at 30 stations ranging from 90° S–82° N. The run began with a spin-up from globally-uniform CO_2 at 375 ppm on 1 January 2004.

than our 1990s values (Le Quéré et al., 2009) causing the discrepancy, but we should also note the use of preliminary fossil fuel CO_2 emission data for 2007–2009.

We note that the lines and symbols in Fig. 14 are not expected to coincide since the symbols are point or single pixel measurements, while the lines are zonal averages. Figure 14 highlights the reduced latitudinal gradient at a higher altitude in the model (also shown in Fig. 11), in which there is actually higher annually-averaged CO_2 at 5 km than at the surface south of ∼ 20° S. The pole-to-pole CO_2 differences can be closely approximated by the Alert (82.45° N) to South Pole (90° S) differences which are summarized in Table 4, along with Mauna Loa (19.5° N) to South Pole differences. While the run without the chemical source persistently overestimates both the Mauna Loa and Alert offsets, the chemical source has some higher offsets and occasional lower offsets, with consistently better offsets at Mauna Loa. This highlights the fact that although both simulations drift to high CO_2 in the NH, skewing the latitudinal gradient, the problem is reduced with the chemical source.

3.2 Vertical profile comparisons

The GLOBALVIEW-CO_2 data set contains some limited measurements of the vertical structure of CO_2 based on in situ or flask measurements from aircraft at select locations.

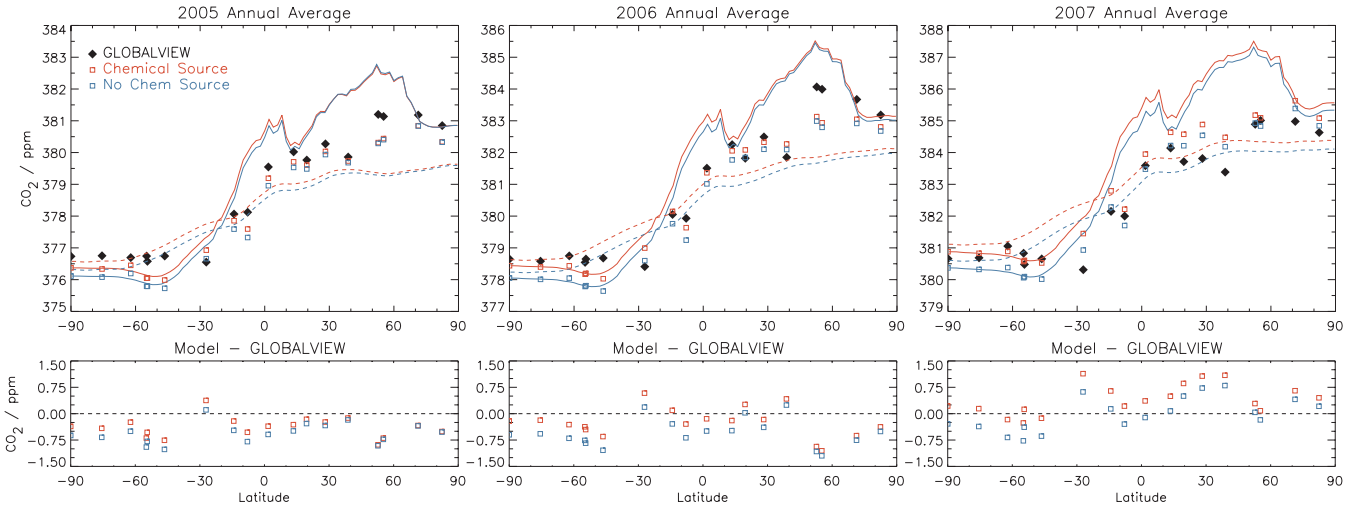

Fig. 14. The upper panels show the annual average CO_2 as a function of latitude for 2005–2007 from GEOS-Chem with the chemical source (red) and without (blue). The zonal average at the surface (solid line) and the zonal average at the model level near 5 km (dotted line) are shown along with single pixels compared with 18 selected GLOBALVIEW stations (black) denoted in Table 3. The lower panels show the model GLOBALVIEW difference at the surface for the two simulations (colored as above), both of which started from a uniform 3-D global CO_2 field of 375 ppm on 1 January 2004.

Table 4. GLOBALVIEW-CO_2 and unconstrained model simulations (with/without chemical source) showing CO_2 (ppm) at the South Pole and the CO_2 offsets at Mauna Loa and Alert relative to the South Pole values.

Year	South Pole			Mauna Loa			Alert		
	GLOBV	Chem	No Chem	GLOBV	Chem	No Chem	GLOBV	Chem	No Chem
2005	376.708	376.370	376.112	+3.21	+3.23	+3.37	+4.11	+3.97	+4.21
2006	378.630	378.437	378.048	+3.23	+3.65	+3.80	+4.53	+4.37	+4.62
2007	380.637	380.878	380.369	+3.22	+3.70	+3.85	+3.97	+4.21	+4.47

Figure 15 shows comparisons of monthly-averaged GEOS-Chem profiles with GLOBALVIEW at a NH coastal site (Estevan Point, BC, Canada), a NH continental site (Park Falls, WI, USA) and a SH remote island site (Rarotonga, Cook Islands, South Pacific Ocean) for 2006. At Estevan Point, the shape and slope of the vertical profile agree very well for most months. In May and June, GLOBALVIEW indicates slightly lower values at the lowest level (0.5 km) than at higher levels (1.5–5.5 km), a feature not present in our model at this location and time but does appear in July–September, when GLOBALVIEW values at 0.5 km have increased. The physical reason for this two-month lag in the model is not known, but it could relate to either CASA or the monthly ocean fluxes, neither of which correspond to an El Niño year like 2006.

At Park Falls, a larger amplitude of variability is observed than at Estevan Point, in both the model and GLOBALVEIW. The general features of the GLOBALVIEW profiles are also reproduced by the model, but at this location from June to September, lower values are observed at the point closest to the surface (1.0 km) than in the model simulation, indicating that the seasonal CO_2 uptake or drawdown in the model is not as strong as in nature. This difference of about 5 ppm can also be observed in the timeseries plots (Fig. 13), and it should be noted that the higher spikes in the model CO_2 timeseries during winter at Park Falls, have little impact on the monthly averages such that the level of agreement during the winter months is high.

At Rarotonga, GEOS-Chem and GLOBALVIEW-CO_2 exhibit different behavior than at the NH sites. The GLOBALVIEW profiles have lower values at the lowest layer (0.5 km) than at all layers above for all months throughout the year. In January, May, June and July, GLOBALVIEW simply increases with altitude up to the top of the profile (4.5 km), but in other months the profile has an inversion at 2.5 or 3.5 km. GEOS-Chem reproduces many of these features such as the positive slope in May–July, but other features like the October inversion or the positive January slope are not reproduced. The underestimate in CO_2 in the free troposphere in January could be due either to excessive drawdown in CO_2 by the climatological biospheric fluxes or insufficient biomass burning emissions,

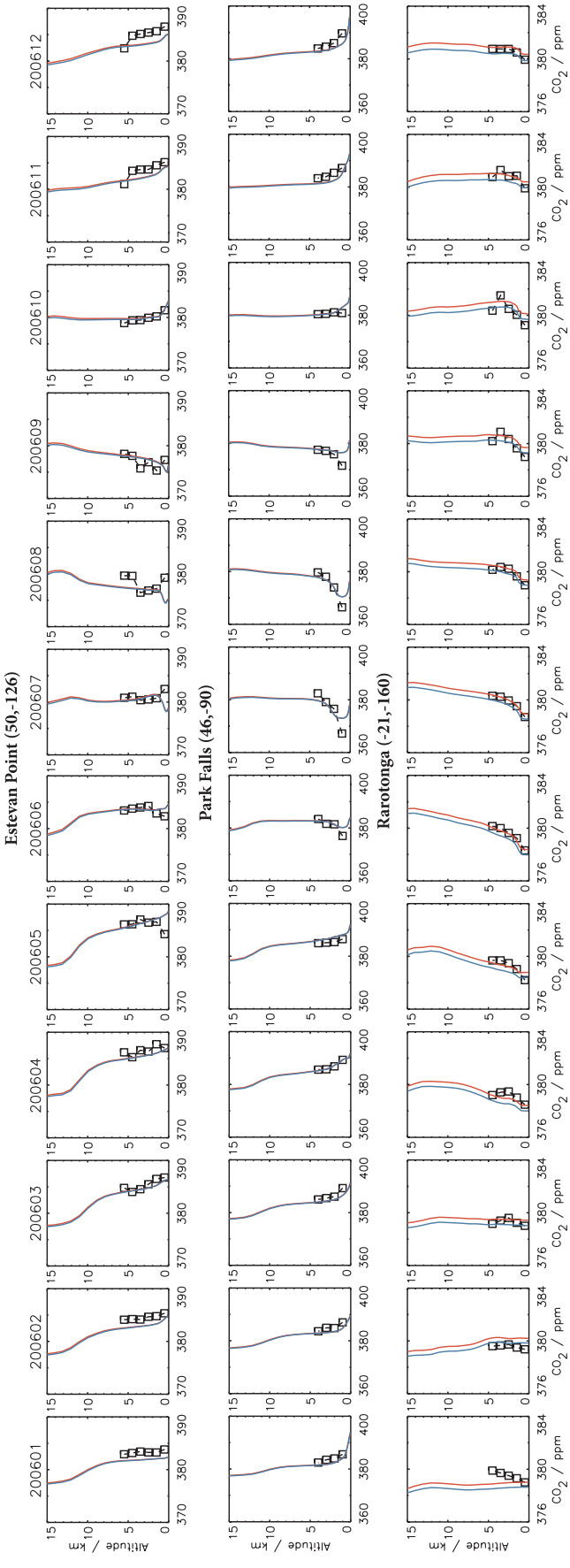

Fig. 15. Comparison of monthly-averaged GEOS-Chem CO_2 vertical profiles (GEOS-5, 47 levels, chemical source in red, no chemical source in blue) and GLOBALVIEW-CO_2 aircraft profiles (black) at a NH coastal site (Estevan Point, BC, Canada), a NH continental site (Park Falls, WI, USA) and a SH remote island site (Rarotonga, Cook Islands, South Pacific Ocean). Note the different x-axis scales required due to the different amplitudes of the seasonal cycle at each location. The chemical source contribution is only distinctly visible for the Rarotonga x-axis range.

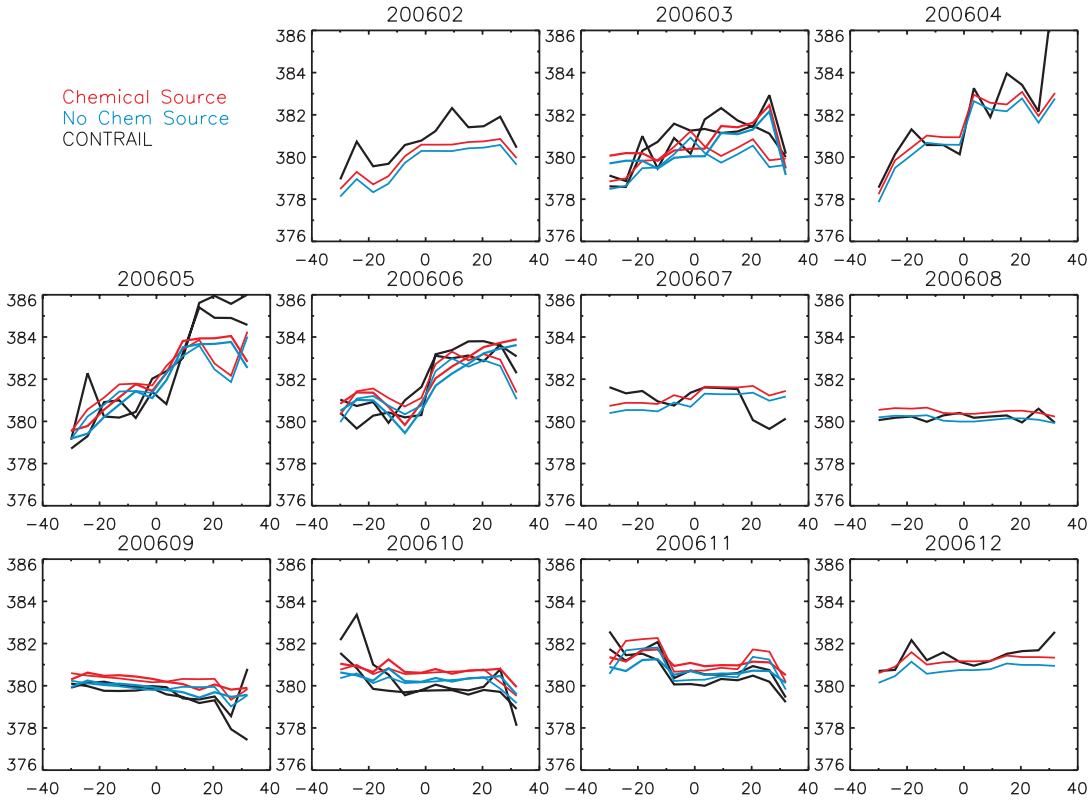

Fig. 16. Comparison of model and CONTRAIL (black) CO_2 (ppm) as a function of latitude for individual flights between Japan and Australia. Model simulations with the chemical source (red) and without it (blue) are sampled at the CONTRAIL locations and times (±3 h). For months with two flights plotted on the same panel, dotted lines denote the second flight.

but identifying the cause would require further investigation. The absolute value of the differences at Rarotonga rarely exceeds 1.0 ppm, since at Rarotonga the range of values at any given level up to 4.5 km never exceeds 2.5 ppm, with surface values ranging by about 1.5 ppm. The range of surface values for NH sites reaches nearly 15 ppm at Estevan Point and nearly 30 ppm at Park Falls, due to the active NH terrestrial biosphere.

At Estevan Point and Park Falls, the sub-ppm impact of the chemical source is not evident on the given x-axes, but differences are evident at Rarotonga. These differences appear as a constant offset for the monthly-averaged profiles indicating that CO_2 from the chemical source perturbation is vertically well-mixed at this remote SH ocean location. This is confirmed by the absence of a difference between the surface and 5 km in the zonal average for the SH in Fig. 9, although the figure suggests that in the NH midlatitudes, differences between the impact of the chemical source at the surface and 5 km often exceed 0.2 ppm. This impact on the vertical gradient in the NH is presumably related to the large chemical source surface corrections applied for fossil fuel and biospheric CO_2 precursors, which occur over land mostly in the NH.

3.3 Comparisons with CONTRAIL aircraft data

In the CONTRAIL (Comprehensive Observation Network for TRace gases by AIrLiner) project (Matsueda et al., 2008; Machida et al., 2008), Japan Airlines commercial aircraft are used for measurements of CO_2 and other trace gas species on flights between Japan (Narita Airport, 35.8° N, 145° E) and Australia (Sydney Airport, 34.0° S, 151° E) (Matsueda et al., 2002). The flights make both continuous direct in situ measurements of CO_2 and also collect flask air samples that are subsequently analyzed in laboratory. The measurements sample the atmosphere at an altitude of 9–13 km, mostly cruising at the upper end of this range with ascent and descent providing the measurements at the lower end of the range.

In Fig. 16, we compare GEOS-Chem CO_2 with 17 CONTRAIL transects in the year 2006, with the model sampled at the CONTRAIL flask sample collection locations and times (within ±3 h). The model and CONTRAIL transects typically differ by less than 1 ppm, with only a few exceptions. For 2006, there are 1–2 CONTRAIL transects for most months, although January had none. Differences between the model and CONTRAIL are slightly larger at higher latitudes, likely with some contribution from ascent

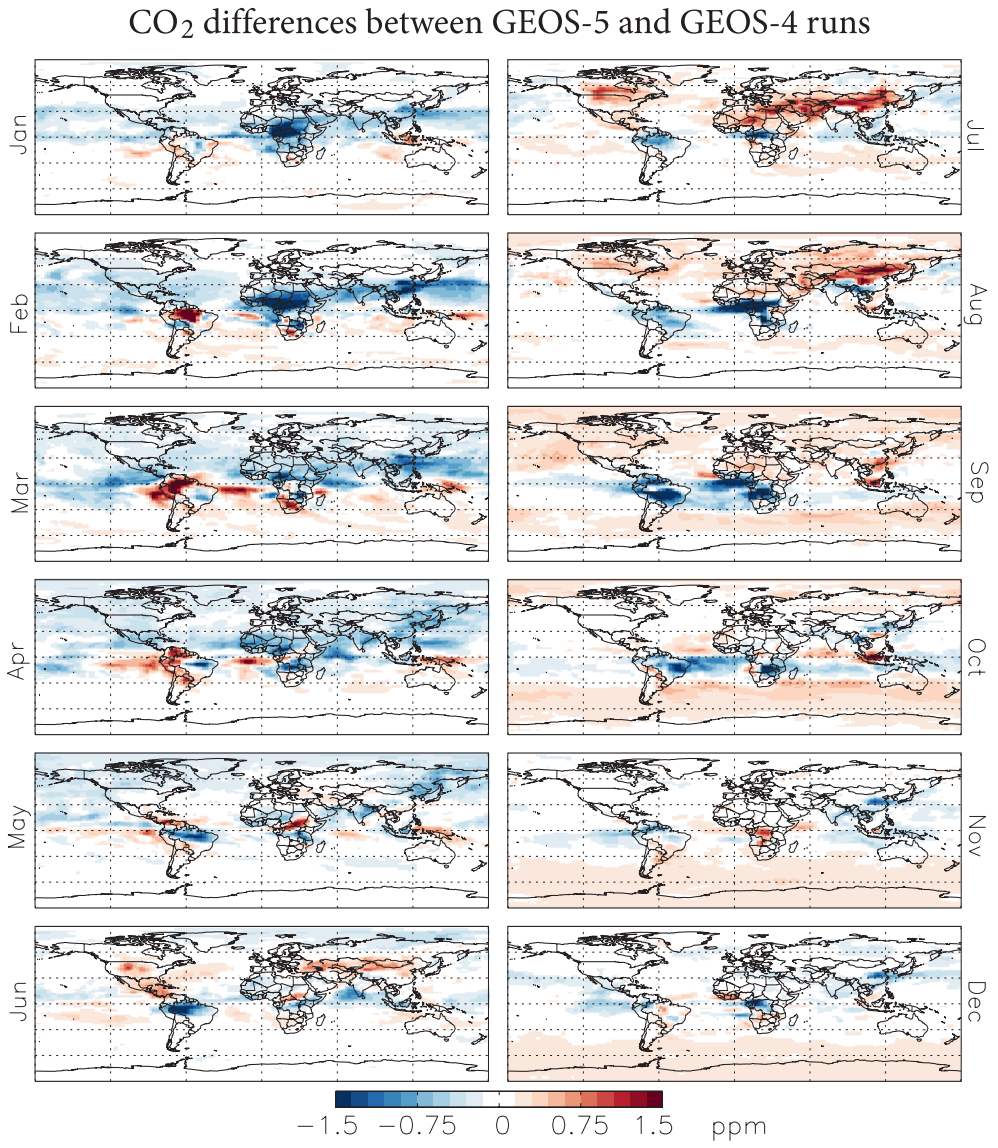

Fig. 17. Monthly-averaged CO_2 difference plots from simulations with different meteorological fields (GEOS-5 and GEOS-4) for 2006 at the level near 5 km. The runs began on 1 January 2004 with identical conditions and were exposed to identical fluxes (without the chemical source).

and descent sampling lower levels of the atmosphere or low CO_2 from stratospheric air, which has more influence at this height at higher latitudes (Sawa et al., 2008). Furthermore, the measured CONTRAIL transects are influenced by temporal variability of the atmosphere on short time scales, that may not be adequately represented by sampling the model within ±3 h. Interestingly, model agreement from February to July was not as good as in the remainder of the year. This may relate to the impact of (NH) springtime biomass burning in south Asia and heightened Asian pollution outflow. Another potential explanation is that better agreement occurs at times of less convection, which would be the case in late 2006 since convection in this region was suppressed due to El Niño (Nassar et al., 2009). This concept is highlighted by Fig. 17, which compares monthly-averaged model CO_2 near 5 km obtained from GEOS-Chem runs for 2006 with two different versions of the meteorological fields (GEOS-4 and GEOS-5), but identical in all other respects. The most significant difference between GEOS-4 and GEOS-5 is their convective parameterization, since GEOS-4 uses the Zhang-McFarlane convection scheme (Zhang and McFarlane, 1995) and GEOS-5 uses the Relaxed Arakawa-Schubert scheme (Moorthi and Suarez, 1992). Figure 17 reveals that the largest differences between the GEOS-4 and GEOS-5 CO_2 runs occur over tropical land regions, which are regions that exhibit some of the strongest

convective uplifting. Quantification of model transport errors related to convection will be an important topic in future CO_2 inverse modeling studies. Both aircraft measurements of CO_2 and satellite observations of CO_2 (given some time to mature) will be valuable for evaluating model transport errors of this nature. Further comparisons of our GEOS-Chem CO_2 simulations with aircraft observations were carried out for the HIAPER Pole-to-Pole Observations (HIPPO) campaigns of 2009 (Wofsy et al., 2010), although biomass burning and fossil fuel emission inventory values for 2009 were not available for that work.

4 Discussion and conclusions

We have used the GEOS-Chem CO_2 simulation with CO_2 emissions from global monthly-varying fossil fuel use, shipping, aviation and the chemical production of CO_2 from the oxidation of reduced carbon species. This makes GEOS-Chem one of the first global models to include a detailed accounting of CO_2 emissions from both shipping and aviation, which represent ∼4% of global fossil fuel use and have unique spatial patterns that impact the local structure of the CO_2 distribution, as well as vertical and latitudinal gradients. To our knowledge, this implementation of the chemical source of CO_2 from the oxidation of CO, CH_4 and NMVOCs, and the necessary surface correction is the most comprehensive online representation in a global 3-D CO_2 transport model. We demonstrate that these model modifications have clear impacts on spatial patterns and latitudinal gradients. At the end of a 4-year simulation, the accumulated impact of the shipping and aviation emissions with the chemical source of CO_2 contribute to an increase the global CO_2 latitudinal gradient by just over 0.1 ppm (∼3%), while the inclusion of CO_2 chemical production (and the surface correction) is shown to decrease the latitudinal gradient by about 0.40 ppm (∼10%) with a complex spatial structure generally resulting in decreased CO_2 over land and increased CO_2 over the oceans. In subsequent work, we assess the impact of these new inventories on inverse modeling estimates of CO_2 fluxes using CO_2 satellite observations from TES (Nassar et al., 2010).

In this work we have deliberately focused our model improvement efforts on better representing emissions related to fossil fuel use (including shipping, aviation, and chemical production related to emission of CO_2 precursors) rather than on biospheric fluxes, since CO_2 inverse modeling studies typically accept the fossil fuel inventories, while optimizing biospheric fluxes (which have much larger uncertainties). In order to properly optimize biospheric sources/sinks during assimilation, other significant sources and sinks should be included in the forward model. Inverse modeling results which attempt to constrain the global CO_2 net sink (∼4 Pg C yr^{-1}) on regional scales or smaller based on simulations that have omitted representation of shipping (∼0.19 Pg C yr^{-1}) and aviation (∼0.16 Pg C yr^{-1}), and misrepresented the spatial distribution of CO_2 chemical production (∼1.1 Pg C yr^{-1}), may all have biases since these sources will somehow be compensated for in an unrealistic manner. As a result of uncertainties in the spatio-temporal distribution of the reduced carbon sources and the challenge of accurately accounting for the non-respiratory carbon represented in the balanced biospheric fluxes, the use of the updated model for inverse modeling of atmospheric CO_2 will produce CO_2 flux estimates that additionally incorporate a small residual component primarily accounting for reduced carbon emissions from biospheric combustion processes. We note, however, that these estimates will represent a significant improvement over previous inversion analyses, as the new inventories eliminate most of the systematic error introduced through misallocation of the reduced carbon contribution to atmospheric CO_2. In future work we will investigate other sources of bias associated with the coarse model resolution and the simplified representation of annual terrestrial uptake as we move to higher spatial resolution and explore coupling the GEOS-Chem CO_2 simulation with a terrestrial biospheric model.

Although the global annual mean differences in the CO_2 chemical production rates obtained from the free running model and the CO assimilation were small, the large seasonal differences demonstrate the utility of incorporating ancillary observations to reduce potential bias that could impact the inverse modeling of atmospheric CO_2. Our estimate of 1.18 Pg C yr^{-1} for the chemical source of CO_2 from the assimilation of TES CO represents the first observation-based estimate of this source. With the recent availability of satellite observations of CO, CH_4 and CO_2 from instruments such as TES and others, the approach presented here suggests that assimilation of these species together would provide a more accurate estimate of the atmospheric carbon budget, which would enable us to more reliably quantify the exchange of carbon between the surface and the atmosphere.

Acknowledgements. Work at the University of Toronto was funded by the Natural Sciences and Engineering Research Council (NSERC) of Canada. Work at the Jet Propulsion Laboratory California Institute of Technology was carried out under contract to NASA. We thank all those who have contributed measurements to GLOBALVIEW-CO_2 and thank NOAA-ESRL for making GLOBALVIEW as well as their direct measurement datasets publicly available.

Edited by: M. Kawamiya

References

Andreae, M. O. and Merlet, P.: Emission of trace gases and aerosols from biomass burning, Global Biogeochem. Cy., 15(4), 955–966, 2001.

Andres, R. J., Marland, G., Fung, I., and Matthews, E.: A $1° \times 1°$ distribution of carbon dioxide emissions from fossil fuel consumption and cement manufacture, Global Biogeochem. Cy., 10, 419–429, 1996.

Andres, R. J., Gregg, J. S., Losey, L., Marland, G., and Boden, T. A.: Monthly, global emissions of carbon dioxide from fossil fuel consumption, Tellus B, in revision, 2010.

Baker, D. F.: Sources and Sinks of Atmospheric CO_2 Estimated from Batch Least-Squares Inversions of CO_2 Concentration Measurements, Ph.D. Thesis, Princeton University, 2001.

Baker, D. F., Law, R. M., Gurney, K. M., Rayner, P. Peylin, P. Denning, A. S., Bousquet, P., Bruhwiler, L., Chen, Y.-H., Ciais, P., Fung, I. Y., Heimann, M., John, J., Maki, T., Maksyutov, S., Masarie, K., Prather, M., Pak, B., Taguchi, S., and Zhu, Z.: TransCom 3 inversion intercomparison: Impact of transport model errors on the interannual variability of regional CO_2 fluxes, 1988-2003, Global Biogeochem. Cy., 20, GB1002, doi:10.1029/2004GB002439, 2006.

Bey, I., Jacob, D. J., Yantosca, R. M., Logan, J. A., Field, B. D., Fiore, A. M., Li, Q. B., Liu, H. G. Y., Mickley, L. J., and Schultz, M. G.: Global modeling of tropospheric chemistry with assimilated meteorology: Model description and evaluation, J. Geophys. Res., 106(D19), 23073–23095, 2001.

Chahine, M., Barnet, C., Olsen, E. T., Chen, L., and Maddy, E.: On the determination of atmospheric minor gases by the method of vanishing partial derivatives with application to CO_2, Geophys. Res. Lett., 32, L22803, doi:10.1029/2005GL024165, 2005.

Chahine M. T., Chen, L., Dimotakis, P., Jiang, X., Li, Q., Olsen, E. T., Pagano, T., Randerson, J., and Yung, Y. L.: Satellite remote sounding of mid-tropospheric CO_2, Geophys. Res. Lett., 35, L17807, doi:10.1029/2008GL035022, 2008.

Chan, D., Ishizawa, M., Higuchi, K., Maksyutov, S., and Chen, J.: Seasonal CO_2 rectifier effect and large-scale extratropical atmospheric transport, J. Geophys. Res., 113, D17309, doi:10.1029/2007JD009443, 2008.

Chevallier, F., Breon, F.-M., and Rayner, P. J.: Contribution of the Orbiting Carbon Observatory to the estimation of CO_2 sources and sins: Theoretical study in a variational data assimilation framework, J. Geophys. Res., 112, D09307, doi:10.1029/2006JD007375, 2007.

Ciais, P., Borges, A. V., Abril, G., Meybeck, M., Folberth, G., Hauglustaine, D., and Janssens, I. A.: The impact of lateral carbon fluxes on the European carbon balance, Biogeosciences, 5, 1259–1271, doi:10.5194/bg-5-1259-2008, 2008.

Cole, J. J., Prairie, Y. T., Caraco, N. F., McDowell, W. H., Tranvik, L. J., Streigl, R. G., Duarte, C. M., Kortelainen, P., Downing, J. A., Middelburg, J. J., and Melack, J.: Plumbing the global carbon cycle: Integrating inland waters into the terrestrial carbon budget, Ecosystems, 10, 171–184, 2007.

Corbett, J. J. and Koehler, H. W.: Updated emissions from ocean shipping, J. Geophys. Res., 108(D20), 4650, doi:10.1029/2003JD003751, 2003.

Corbett, J. J. and Koehler, H. W.: Considering alternative input parameters in an activity-based ship fuel consumption and emissions model: Reply to comment by Øyvind Endresen et al. on "Updated emissions from ocean shipping", J. Geophys. Res., 109, D23303, doi:10.1029/2004JD005030, 2004.

Crevoisier, C., Chédin, A., Matsueda, H., Machida, T., Armante, R., and Scott, N. A.: First year of upper tropospheric integrated content of CO_2 from IASI hyperspectral infrared observations, Atmos. Chem. Phys., 9, 4797–4810, doi:10.5194/acp-9-4797-2009, 2009.

Denman, K. L. Brasseur, G., Chidthiasong, A., Ciais, P., Cox, P. M., Dickenson, R. E., Huaglustaine, D., Heinze, C., Holland, E., Jacob, D., Lohmann, U., Ramachandran, S., da Silva Dias, P. L., Wofsy, S. C., and Zhang, X.: Couplings between changes in the Climate System and Biogeochemistry, in: Climate Change 2007: The Physical Science Basis. Contribution of Working Group I to the fourth Assessment Report of the Intergovernmental Panel on Climate Change (IPCC), edited by: Solomon, S., Qin, D., Manning, Z., Chen, M., Marquis, M., Averyt, K. B., Tignor, M., and Miller, H. L., Cambridge University Press, Cambridge, UK and New York, NY, USA, 996 pp., 2007.

Denning, A. S., Fung, I. Y., and Randall, D. A.: Gradient of atmospheric CO_2 due to seasonal exchange with land biota, Nature, 376, 240–243, 1995.

Duncan, B. N., Martin, R. V., Staudt, A. C., Yevich, R., and Logan, J. A.: Interannual and seasonal variability of biomass burning emissions constrained by satellite observations, J. Geophys. Res., 108(D2), 4100, doi:10.1029/2002JD002378, 2003.

Endresen, Ø., Sørgård, E., Bakke, J., and Isaksen, I. S. A.: Substantiation of a lower estimate for the bunker inventory: Comment on "Updated emissions from ocean shipping" by James J. Corbett and Horst W. Koehler, J. Geophys. Res., 109, D23302, doi:10.1029/2004JD004853, 2004.

Endresen, Ø., Sørgärd, E., Behrens, H. L., Brett, P. O., Isaksen, I. S. A.: A historical reconstruction of ships fuel consumption and emissions, J. Geophys. Res., 112, D12301, doi:10.1029/2006JD007630, 2007.

Enting, I. G.: Inverse Problems in Atmospheric Constituent Transport, Cambridge University Press, Cambridge, 2002.

Enting, I. G. and Mansbridge, J. V.: Latitudinal distribution of sources and sinks of CO_2: Results of and inversion study, Tellus B, 43, 156–170, 1991.

Enting, I. G., Trudinger, C. M., and Francey, R. J.: A synthesis inversion of the concentration and δ^{13}C of atmospheric CO_2, Tellus B, 47, 35–52, 1995.

Eyring, V., Isaksen, I. S. A, Berntsen, T., Collins, W. J., Corbett, J. J., Endresen, O., Grainger, R. G., Moldanova, J., Schlager, H., and Stevenson, D. S.: Transport impacts on atmosphere and climate: Shipping, Atmos. Environ., 44, 4735–4771, doi:10.1016/j.atmosenv.2009.04.059, 2010.

Feng, L., Palmer, P. I., Bösch, H., and Dance, S.: Estimating surface CO_2 fluxes from space-borne CO_2 dry air mole fraction observations using an ensemble Kalman Filter, Atmos. Chem. Phys., 9, 2619–2633, doi:10.5194/acp-9-2619-2009, 2009.

Feng, L., Palmer, P. I., Yang, Y., Yantosca, R. M., Kawa, S. R., Paris, J.-D., Matsueda, H., and Machida, T.: Evaluating a 3-D transport model of atmospheric CO_2 using ground-based, aircraft, and space-borne data, Atmos. Chem. Phys. Discuss., 10, 18025–18061, doi:10.5194/acpd-10-18025-2010, 2010.

Folberth, G., Hauglustaine, D. A., Ciais, P., and Lathiére, J.: On the role of atmospheric chemistry in the global CO_2 budget, Geophys. Res. Lett., 32, L08801, doi:10.1029/2004GL021812, 2005.

Folkins, I., Bernath, P., Boone, C., Eldering, A., Lesins, G., Martin, R. V., Sinnhuber, B.-M., and Walker, K.: Testing convective parameterizations with tropical measurements of HNO_3, CO, H_2O, and O_3: Implications for the water vapor budget, J. Geophys. Res., 111, D23304, doi:10.1029/2006JD007325, 2006.

Friedl, R. R. (Ed.): Atmospheric Effects of Subsonic Aircraft: Interim Assessment Report of the Advanced Subsonic Technology Program, Ref. Publ. 1400, NASA, Greenbelt, Md., 168 pp., 1997.

Friedlingstein, P., Houghton, R. A., Marland, G., Hackler, J., Boden, T. A., Conway, T. J., Canadell, J. G., Raupach, M. R., Ciais, P., and Le Quéré, C.: Update on CO_2 emissions, Nat. Geosci., 3, 811–812, doi:10.1038/ngeo1022, 2010.

Gerbig, C., Lin, J. C., Wofsy, S. C., Daube, B. C., Andrews, A. E., Stephens, B. B., Bakwin, P. S., and Grainger, C. A.: Toward constraining regional-scale fluxes of CO_2 with atmospheric observations over a continent: 1. Observed spatial variability from airborne platforms, J. Geophys. Res., 108(D24), 4756, doi:10.1029/2002JD003018, 2003a.

Gerbig, C., Lin, J. C., Wofsy, S. C., Daube, B. C., Andrews, A. E., Stephens, B. B., Bakwin, P. S., and Grainger, C. A.: Toward constraining regional-scale fluxes of CO_2 with atmospheric observations over a continent: 2. Analysis of COBRA data using a receptor-oriented framework, J. Geophys. Res., 108(D24), 4757, doi:10.1029/2003JD003770, 2003b.

Giglio, L., Descloitres, J., Justice, C. O., and Kaufman, Y. J.: An enhanced contextual fire detection algorithm for MODIS, Remote Sen. Environ., 87(2–3), 273–282, 2003.

GLOBALVIEW-CO_2: Cooperative Atmospheric Data Integration Project – Carbon Dioxide, CD-ROM, NOAA ESRL, Boulder, Colorado, available via anonymous FTP to ftp.cmdl.noaa.gov, Path: ccg/co2/GLOBALVIEW, 2009.

Gloor, M., Sarmiento, J. L., and Gruber, N.: What can be learned about carbon cycle climate feedbacks from the CO2 airborne fraction?, Atmos. Chem. Phys., 10, 7739–7751, doi:10.5194/acp-10-7739-2010, 2010.

Gregg, J. S., Andres, R. J., and Marland, G.: China: Emissions pattern of the world leader in CO_2 emissions from fossil fuel consumption and cement production, Geophys. Res. Lett., 35, L08806, doi:10.1029/2007GL032887, 2008.

Guenther, A.: Corrigendum to "Estimates of global terrestrial isoprene emissions using MEGAN (Model of Emissions of Gases and Aerosols from Nature)" published in Atmos. Chem. Phys., 6, 3181–3210, 2006, Atmos. Chem. Phys., 7, 4327–4327, doi:10.5194/acp-7-4327-2007, 2007.

Guenther, A., Karl, T., Harley, P., Wiedinmyer, C., Palmer, P. I., and Geron, C.: Estimates of global terrestrial isoprene emissions using MEGAN (Model of Emissions of Gases and Aerosols from Nature), Atmos. Chem. Phys., 6, 3181–3210, doi:10.5194/acp-6-3181-2006, 2006.

Gurney, K. R., Law, R. M., Denning, A. S., Rayner, P. J., Baker, D., Bousquet, P., Bruhwiler, L., Chen, Y. H., Ciais, P., Fan, S.-M., Fung, I. Y., Gloor, M., Heimann, M., Higuchi, K., John, J., Kowalczyk, E., Maki, T., Maksyutov, S., Peylin, P., Prather, M., Pak, B. C., Sarmiento, J. L., Taguchi, S., Takahashi, T., and Yuen, C. W.: TransCom 3 CO_2 inversion intercomparison: 1. Annual mean control results and sensitivity to transport and prior flux information, Tellus B, 55, 555–579, 2003.

Houweling, S., Breon, F.-M., Aben, I., Rödenbeck, C., Gloor, M., Heimann, M., and Ciais, P.: Inverse modeling of CO_2 sources and sinks using satellite data: a synthetic inter-comparison of measurement techniques and their performance as a function of space and time, Atmos. Chem. Phys., 4, 523–538, doi:10.5194/acp-4-523-2004, 2004.

Houweling, S., Aben, I., Breon, F.-M., Chevallier, F., Deutscher, N., Engelen, R., Gerbig, C., Griffith, D., Hungershoefer, K., Macatangay, R., Marshall, J., Notholt, J., Peters, W., and Serrar, S.: The importance of transport model uncertainties for the estimation of CO_2 sources and sinks using satellite measurements, Atmos. Chem. Phys., 10, 9981–9992, doi:10.5194/acp-10-9981-2010, 2010.

Jacobson, A. R., Mikaloff Fletcher, S. E., Gruber, N., Sarmiento, J. L., and Gloor, M.: A joint atmosphere-ocean inversion for surface fluxes of carbon dioxide: 1. Methods and global-scale fluxes, Global Biogeochem. Cy., 21, GB1019, doi:10.1029/2005GB002556, 2007a.

Jacobson, A. R., Mikaloff Fletcher, S. E., Gruber, N., Sarmiento, J. L., and Gloor, M.: A joint atmosphere-ocean inversion for surface fluxes of carbon dioxide: 2. Regional results, Global Biogeochem. Cy., 21, GB1020, doi:10.1029/2006GB002703, 2007b.

Kadygrov, N., Maksyutov, S., Eguchi, N., Aoki, T., Nakazawa, T., Yokota, T. and Inoue, G.: Role of simulated GOSAT total column CO_2 observations in surface CO_2 flux uncertainty reduction, J. Geophys. Res., 114, D21208, doi:10.1029/2008JD011597, 2009.

Keeling, C. D.: The Concentration and Isotopic Abundances of Carbon Dioxide in the Atmosphere, Tellus, 12(2), 200–203, 1960.

Keeling, C. D., Bacastow, R. B., Carter, A. F., Piper, S. C., Whorf, T. P., Heimann, M., Mook, W. G., Roeloffzen, H.: A three-dimensional model of atmospheric CO_2. Transport based on observed winds 1: Analysis of observational data, in: Aspects of Climate Variability in the Pacific and Western Americas, edited by: Peterson, D. H., American Geophysical Union, Washington, DC, Geophys. Monogr. 55, 165–236, 1989.

Keeling, C. D., Piper, S. C., and Whorf, T. P.: A 50 year record of the evolution of the meridional gradient in atmospheric CO_2 and its relation to fossil fuel emissions, Proceedings of the International Carbon Dioxide Conference (ICDC), 2005.

Kim, B., Fleming, G., Balasubramanian, S., Malwitz, A., Lee, J., Waitz, I., Klima, K., Locke, M., Holsclaw, C., Morales, A., McQueen, E., and Gillette, W.: System for assessing Aviation's Global Emissions (SAGE) Federal Aviation Administration Office of Environment and Energy, Version 1.5, Global Aviation Emissions Inventories for 2000 through 2004 (FAA-EE-2005-02), September 2005.

Kim, B. Y., Fleming, G. G., Lee, J. J., Waitz, I. A., Clarke, J.-P., Balasubramanian, S., Malwitz, A., Klima, K., Locke, M., Holsclaw, C. A., Maurice, L. Q., and Gupta, M. L.: System for assessing Aviation's Global Emissions (SAGE), Part 1: Model description and inventory results, Transport. Res. D-TRE, 12, 325–346, 2007.

Kopacz, M., Jacob, D. J., Fisher, J. A., Logan, J. A., Zhang, L., Megretskaia, I. A., Yantosca, R. M., Singh, K., Henze, D. K., Burrows, J. P., Buchwitz, M., Khlystova, I., McMillan, W. W., Gille, J. C., Edwards, D. P., Eldering, A., Thouret, V., and Nedelec, P.: Global estimates of CO sources with high resolution by adjoint inversion of multiple satellite datasets (MOPITT, AIRS, SCIAMACHY, TES), Atmos. Chem. Phys., 10, 855–876, doi:10.5194/acp-10-855-2010, 2010.

Kulawik, S. S., Jones, D. B. A., Nassar, R., Irion, F. W., Worden, J. R., Bowman, K. W., Machida, T., Matsueda, H., Sawa, Y., Biraud, S. C., Fischer, M. L., and Jacobson, A. R.:

Characterization of Tropospheric Emission Spectrometer (TES) CO_2 for carbon cycle science, Atmos. Chem. Phys., 10, 5601–5623, doi:10.5194/acp-10-5601-2010, 2010.

Law, R. M., Rayner, P. J., Denning, A. S., Erickson, D., Fung, I. Y., Heimann, M., Piper, S. C., Romonet, M., Taguchi, S., Taylor, J. A., Trudinger, C. M., and Watterson, I. G.: Variations in modeled atmospheric transport of carbon dioxide and the consequences for CO_2 inversions, Global Biogeochem. Cy., 10(4), 783–796, 1996.

Le Quéré, C., Raupach, M. R., Canadell, J. G., Marland, G., Bopp, L., Ciais, P., Conway, T. J., Doney, S. C., Feely, R. A., Foster, P., Friedlingstein, P., Gurney, K., Houghton, R. A., House, J. I., Huntingford, C., Levy, P. E., Lomas, M. R., Majkut, J., Metzl, N., Ometto, J. P., Peters, G. P., Prentice, I. C., Randerson, J. T., Running, S. W., Sarmiento, J. L., Schuster, U., Sitch, S., Takahashi, T., Viovy, N., van der Werf, G. R., and Woodward, F. I.: Trends in the sources and sinks of carbon dioxide, Nat. Geosci., 2, 831–836, doi:10.1038/ngeo689, 2009.

Li, Q., Jacob, D. J., Munger, J. W., Yantosca, R. M., and Parrish, D. D.: Export of NOy from the North American boundary layer: Reconciling aircraft observations and global model budgets, J. Geophys. Res., 109, D02313, doi:10.1029/2003JD004086, 2004.

Machida, T., Matsueda, H., Sawa, Y., Nakagawa, Y., Hirotani, K., Kondo, N., Goto, K., Nakazawa, T., Ishikawa, K., and Ogawa, T.: Worldwide measurements of atmospheric CO_2 and other trace gas species using commercial airlines, J. Atmos. Ocean. Tech., 25(10), 1744–1754, 2008.

Marland, G. and Rotty, R. M.: Carbon Dioxide Emissions from fossil fuels: A procedure for estimation and results for 1950–1982, Tellus B, 36, 232–261, 1984.

Masarie, K. A. and Tans, P. P.: Extension and integration of atmospheric carbon dioxide data into a globally consistent measurement record, J. Geophys. Res., 100(D6), 115993–11610, 1995.

Matsueda, H., Inoue, H. Y., and Ishii, M.: Aircraft observation of carbon dioxide at 8–13 km altitude over the Western Pacific from 1993 to 1999, Tellus B, 54(1), 1–21, 2002.

Matsueda, H., Machida, T., Sawa, Y., Nakagawa, Y., Hirotani, K., Ikeda, H., Kondo, N., and Goto, K.: Evaluation of atmospheric CO_2 measurements from new flask air sampling of JAL airliner observation, Pap. Meteorol. Geophys., 59, 1–17, 2008.

Miller, C. E., Crisp, D., DeCola, P. L., Olsen, S. C., Randerson, J. T., Michalak, A. M., Alkhaled, A., Rayner, P., Jacob, D. J., Suntharalingam, P., Jones, D. B. A., Denning, A. S., Nicholls, M. E., Doney, S. C., Pawson, S., Boesch, H., Connor, B. J., Fung, I. Y., O'Brien, D., Salawitch, R. J., Sander, S. P., Sen, B., Tans, P., Toon, G. C., Wennberg, P. O., Wofsy, S. C., Yung, Y. L., and Law, R. M.: Precision requirements for space-based X_{CO_2} data, J. Geophys. Res., 112(D10), D10314, doi:10.1029/2006JD007659, 2007.

Millet, D. B., Guenther, A., Siegel, D. A., Nelson, N. B., Singh, H. B., de Gouw, J. A., Warneke, C., Williams, J., Eerdekens, G., Sinha, V., Karl, T., Flocke, F., Apel, E., Riemer, D. D., Palmer, P. I., and Barkley, M.: Global atmospheric budget of acetaldehyde: 3-D model analysis and constraints from in-situ and satellite observations, Atmos. Chem. Phys., 10, 3405–3425, doi:10.5194/acp-10-3405-2010, 2010.

Moorthi, S. and Suarez, M.: Relaxed Arakawa-Schubert: A parameterization of moist convection for general circulation models, Mon. Weather Rev., 120, 978–1002, 1992.

Nassar, R., Logan, J. A., Megretskaia, I. A., Murray, L. T., Zhang, L., and Jones, D. B. A.: Analysis of tropical tropospheric ozone, carbon monoxide and water vapor during the 2006 El Niño using TES observations and the GEOS-Chem model, J. Geophys. Res., 114, D17304, doi:10.1029/2009JD011760, 2009.

Nassar, R., Jones, D. B. A., Kulawik, S. S., Worden, J. R., Bowman, K. W., Brenninkmeijer, C. A., Schuck, T. J., Conway, T. J., and Worthy, D. E.: Inverse modeling of CO_2 sources and sinks using satellite observations of CO_2 from TES and surface flask measurements, Atmos. Chem. Phys., in preparation, 2010.

Olivier, J. G. J. and Berdowski, J. J. M: Global emissions sources and sinks, in: The Climate System, edited by: Berdowski, J., Guicherit, R., and Heij, B. J., A. A. Balkema Publishers/Swets and Zeitlinger Publishers, Lisse, The Netherlands, 33–78, 2001.

Olsen, S. C. and Randerson, J. T.: Differences between surface and column atmospheric CO_2 and implications for carbon cycle research, J. Geophys. Res., 109, D02301, doi:10.1029/2003JD003968, 2004.

Pak, B. C. and Prather, M. J.: CO_2 source inversions using satellite observations of the upper troposphere, Geophys. Res. Lett., 28(24), 4571–4574, 2001.

Palmer, P. I., Suntharalingham, P., Jones, D. B. A., Jacob, D. J., Streets, D. G., Fu, Q., Vay, S., and Sachse, G. W.: Exploiting observed CO:CO_2 correlations to improve inverse analyses of carbon fluxes, J. Geophys. Res., 111, D12318, doi:10.1029/2005JD006697, 2006.

Palmer, P. I., Barkley, M. P., and Monks, P. S.: Interpreting the variability of space-borne CO_2 column-averaged volume mixing ratios over North America using a chemistry transport model, Atmos. Chem. Phys., 8, 5855–5868, doi:10.5194/acp-8-5855-2008, 2008.

Parrington, M., Jones, D. B. A., Bowman, K. W., Horowitz, L. W., Thompson, A. M., Tarasick, D. W., and Witte, J. C.: Estimating the summertime tropospheric ozone distribution over North America through assimilation of observations from the Tropospheric Emission Spectrometer, J. Geophys. Res., 113, D18307, doi:10.1029/2007JD009341, 2008.

Pillai, D., Gerbig, C., Marshall, J., Ahmadov, R., Kretschmer, R., Koch, T., and Karstens, U.: High resolution modeling of CO_2 over Europe: implications for representation errors of satellite retrievals, Atmos. Chem. Phys., 10, 83–94, doi:10.5194/acp-10-83-2010, 2010.

Potter, C. S., Randerson, J. T., Field, C. B., Matson, P. A., Vitousek, P. M., Mooney, H. A., and Klooster, S. A.: Terrestrial ecosystem production: A process model based on global satellite and surface data, Global Biogeochem. Cy., 7, 811–841, 1993.

Randerson, J. T., Chapin III, F. S., Harden, J. W., Neff, J. C., and Harmon, M. E.: Net Ecosystem Production: A Comprehensive Measure of Net Carbon Accumulation by Ecosystems, Ecol. Appl., 12(4), 937–947, 2002.

Rayner, P. J. and O'Brien, D. M.: The utility of remotely sensed CO_2 concentration data in surface source inversions, Geophys. Res. Lett., 28(1), 175–178, 2001.

Sausen, R. and Schumann, U.: Estimates of the Climate Response to Aircraft CO_2 and NO_x Emissions Scenarios, Climate Change, 44, 27–58, 2000.

Sawa, Y., Machida, T., and Matsueda, H.: Seasonal variations of CO_2 near the tropopause observed by commercial aircraft, J. Geophys. Res., 113, D23301, doi:10.1029/2008JD010568, 2008.

Suntharalingam, P., Spivakovsky, C. M., Logan, J. A., and McElroy, M. B.: Estimating the distribution of terrestrial CO_2 sources and sinks from atmospheric measurements: Sensitivity to configuration of the observation network, J. Geophys. Res., 108(D15), 4452, doi:10.1029/2002JD002207, 2003.

Suntharalingam, P., Jacob, D. J., Palmer, P. I., Logan, J. A., Yantosca, R. M., Xiao, Y., Evans, M. J., Streets, D. G., Vay, S. L., Sachese, G. W.: Improved quantification of Chinese carbon fluxes using CO_2/CO correlations in Asian outflow, J. Geophys. Res., 109, D18S18, doi:10.1029/2003JD004362, 2004.

Suntharalingam, P., Randerson, J. T., Krakauer, N., Logan, J. A., and Jacob, D. J.: Influence of reduced carbon emissions and oxidation on the distribution of atmospheric CO_2: Implications for inversion analyses, Global Biogeochem. Cy., 19, GB4003, doi:10.1029/2005GB002466, 2005.

Takahashi, T., Feely, R. A., Weiss, R., Wanninkhof, R. H., Chipman, D. W., Sutherland, S. C., and Takahashi, T. T.: Global air-sea flux of CO_2: an estimate based on measurements of sea-air pCO_2 difference, P. Natl. Acad. Sci. USA, 94, 8292–8299, 1997.

Takahashi, T., Sutherland, S. C., Sweeney, C., Poisson, A., Metzl, N., Tillbrook, B., Bates, N., Wanninkhof, R., Feely, R. A., Sabine, C., Olafsson, J., and Nojiri, Y.: Global sea-air CO_2 flux based on climatological surface ocean pCO_2, and seasonal biological and temperature effects, Deep-Sea Res. Pt. II, 49, 1601–1622, 2002.

Takahashi, T., Sutherland, S. C., Wanninkhof, R., Sweeney, C., Feely, A., Chipman, D. W., Hales, B. E., Friederich, G. E., Chavez, F., Sabine, C. L., Watson, A. J., Bakker, D. C. E., Schuster, E., Metzl, N., Yoshikawa-Inoue, H., Ishii, M., Midorikawa, T., Nojiri, Y., Körtzinger, A., Steinhoff, T., Hoppema, M., Olafsson, J., Arnarson, T. S., Tilbrook, B., Johannessen, T., Olsen, A., Bellerby, R., Wong, C. S., Delille, B., Bates, N. R., and de Baar, H. J. W.: Climatological mean and decadal change in surface ocean pCO_2, and net sea-air CO_2 flux over the global oceans, Deep-Sea Res. Pt. II, doi:10.1016/j.dsr2.2008.12.009, 2009.

Taylor, J. A. and Orr, J. C.: The natural latitudinal distribution of atmospheric CO_2, Global Planet. Change, 26, 375-386, 2000.

United Nations: 1984 Demographic Yearbook, Dep. of Int. and Soc. affairs, Stat. Off. New York, 1984.

van der Werf, G. R., Randerson, J. T., Giglio, L., Collatz, G. J., Kasibhatla, P. S., and Arellano Jr., A. F.: Interannual variability in global biomass burning emissions from 1997 to 2004, Atmos. Chem. Phys., 6, 3423–3441, doi:10.5194/acp-6-3423-2006, 2006.

van der Werf, G. R., Randerson, J. T., Giglio, L., Collatz, G. J., Mu, M., Kasibhatla, P. S., Morton, D. C., DeFries, R. S., Jin, Y., and van Leeuwen, T. T.: Global fire emissions and the contribution of deforestation, savanna, forest, agricultural, and peat fires (1997–2009), Atmos. Chem. Phys. Discuss., 10, 16153–16230, doi:10.5194/acpd-10-16153-2010, 2010.

Wang, C., Corbett, J. J., and Firestone, J.: Modeling Energy Use and Emissions from North American Shipping: Application of the Ship Traffic, Energy, and Environment Model, Environ. Sci. Technol. 41, 3226–3232, 2008.

Wang, H., Jacob, D. J., Kopacz, M., Jones, D. B. A., Suntharalingam, P., Fisher, J. A., Nassar, R., Pawson, S., and Nielsen, J. E.: Error correlation between CO_2 and CO as constraint for CO_2 flux inversions using satellite data, Atmos. Chem. Phys., 9, 7313–7323, doi:10.5194/acp-9-7313-2009, 2009.

Wilkerson, J. T., Jacobson, M. Z., Malwitz, A., Balasubramanian, S., Wayson, R., Fleming, G., Naiman, A. D., and Lele, S. K.: Analysis of emission data from global commercial aviation: 2004 and 2006, Atmos. Chem. Phys., 10, 6391–6408, doi:10.5194/acp-10-6391-2010, 2010.

Wofsy, S. C., Daube, B. C., Jimenez, R., Kort, E., Pittman, J. V., Park, S., Commane, R., Xiang, B., Santoni, G., Jacob, D., Fisher, J., Pickett-Heaps, C., Wang, H., Wecht, K., Wang, Q.-Q., Stephens, B. B., Shertz, S., Romashkin, P., Campos, T., Haggerty, J., Cooper, W. A., Rogers, D., Beaton, S., Hendershot, R., Elkins, J. W., Fahey, D. W., Gao, R. S., Moore, F., Montzka, S. A., Schwarz, J. P., Hurst, D., Miller, B., Sweeney, C., Oltmans, S., Nance, D., Hintsa, E., Dutton, G., Watts, L. A., Spackman, J. R., Rosenlof, K. H., Ray, E. A., Zondlo, M. A., Diao, M., Keeling, R., Bent, J., Atlas, E. L., Lueb, R., Mahoney, M. J., Chahine, M., Olsen, E., Patra, P., Ishijima, K., Engelen, R., Nassar, R., Jones, D. B. A., and Mikaloff-Fletcher, S. E.: HIAPER Pole-to-Pole Observations (HIPPO): Fine grained, global scale measurements of climatically important atmospheric gases and aerosols, Proceedings of the Royal Society A, in press, 2010.

Yevich, R. and Logan, J. A.: An assessment of biofuel use and burning of agricultural waste in the developing world, Global Biogeochem. Cy., 17(4), 1095, doi:10.1029/2002GB001952, 2003.

Zhang, G. J. and McFarlane, N. A.: Sensitivity of climate simulations to the parameterization of cumulus convection in the Canadian Climate Centre General Circulation Model, Atmos. Ocean, 33, 407–446, 1995.